



## Article

# Change Analysis on the Spatio-Temporal Patterns of Main Crop Planting in the Middle Yangtze Plain

Luguang Jiang <sup>1,2,\*</sup> , Si Wu <sup>1,2</sup> and Ye Liu <sup>1</sup>

<sup>1</sup> Institute of Geographic Sciences and Natural Resources Research, Chinese Academy of Sciences, Beijing 100101, China; wusi19@mails.ucas.ac.cn (S.W.); liuye.16s@igsrr.ac.cn (Y.L.)

<sup>2</sup> College of Resources and Environment, University of Chinese Academy of Sciences, Beijing 100049, China

\* Correspondence: jianglg@igsrr.ac.cn; Tel.: +86-010-64889471

**Abstract:** As a traditional agricultural production base in China, the Middle Yangtze Plain (MYP) is a typical region to explore the intensification, large-scale, and agglomeration of agricultural land, and its crop planting situation is sensitive to changes in national agricultural policy and economic development. So far, the research of crop remote sensing extraction mainly has focused on the areas with simple crops rotation patterns, by using short-time sequence remote sensing data with low spatial resolution. The objective of this study was to address how to accurately map the spatial distribution of main crops considering their spectral and phenological features, and what characteristics of spatio-temporal patterns dynamics of crops occurred in the MYP in 1990–2020. Based on Landsat and MODIS data, using the Enhanced Spatial and Temporal Adaptive Reflectance Fusion Model (ESTARFM) as well as the raster-based spectral and phenological differential change method (RSPDCM), this study mapped the spatial distribution of main crops (rice, cotton, maize, soybean, rapeseed and winter wheat) in the MYP during 1990–2020 and analyzed their planting characteristics. The RSPDCM has a good overall accuracy of more than 89%. The planting characteristics of the main crops were highly intensive and agglomerate double-cropping rotation in the MYP's paddy field. Rice and rapeseed were the two most important crops, accounting for 74.75% of the annual planting area. The highly intensive and large-scale areas were mainly distributed in the Dongting Lake Plain (DTLP) and Poyang Lake Plain (PYLP), while the highly agglomerate areas of main crops were mainly distributed in the Jiangnan Plain (JHP). This study innovatively provides a high-precision multi-cropping spatial dynamic mapping method and basic information, which is helpful to realize high-precision remote sensing extraction of crops in different regions of the world and provide basic data for optimizing the allocation of agricultural production resources in top grain-producing areas.

**Keywords:** land resource evaluation; remote sensing extraction; Landsat-MODIS fusion data; driving mechanism



**Citation:** Jiang, L.; Wu, S.; Liu, Y. Change Analysis on the Spatio-Temporal Patterns of Main Crop Planting in the Middle Yangtze Plain. *Remote Sens.* **2022**, *14*, 1141. <https://doi.org/10.3390/rs14051141>

Academic Editor: David M. Johnson

Received: 17 January 2022

Accepted: 23 February 2022

Published: 25 February 2022

**Publisher's Note:** MDPI stays neutral with regard to jurisdictional claims in published maps and institutional affiliations.



**Copyright:** © 2022 by the authors. Licensee MDPI, Basel, Switzerland. This article is an open access article distributed under the terms and conditions of the Creative Commons Attribution (CC BY) license (<https://creativecommons.org/licenses/by/4.0/>).

## 1. Introduction

Since the reform and opening up, China's grain demand has grown rapidly, and grain output has risen with fluctuations. Due to the continuous influx of agricultural population into cities to engage in non-agricultural production, the rural labor force has been greatly reduced, aging and weakening, and a large number of high-quality cultivated land has become non-agricultural and non-grain land [1–4]. Moreover, the COVID-19 outbreak has had a dramatic impact on trade and economic aspects of China's food security, and the use of international markets to adjust food supply and demand space has been increasingly limited [5]. China's agricultural production was latent with regional, structural and technical crises, and further ensuring food security faced many challenges [6]. To optimize the regional distribution of crop planting and give full play to the supporting role of main crop planting areas has become an important task to achieve sustainable agricultural development. Rice, wheat, maize, soybean, rapeseed and cotton are the most

important food crops, oil crops and industrial raw materials resources in China, respectively. In the past 30 years, these six crop planting areas accounted for about 60% of the agricultural total area in China [7]. Therefore, in-depth research on the spatio-temporal distribution of main crops in top grain-producing areas was an important basis for promoting agricultural supply-side structural reform and formulating incentive policies.

With the free sharing and rapid development of remote sensing data and its processing methods, establishing the relationship between surface reflection and crops characteristics by using remote sensing data and classification algorithm has gradually become the main method for obtaining crop planting information and generating crop planting area maps [8–10]. At present, remote sensing data for monitoring crops spatial patterns change mainly include low spatial resolution and high temporal resolution data, such as MODIS [11,12] and AVHRR [13], medium spatio-temporal resolution data, such as Landsat [14,15], HJ [16,17] and CBERS [18], and high spatial resolution and low temporal resolution data, such as Sentinel [19], GF [20] and SPOT [21]. In order to achieve large-scale and high-precision extraction of crops spatio-temporal patterns, many agricultural institutions and scholars have begun to explore the fusion of multi-source remote sensing data or remote sensing images with other data [22], such as SPAM (Spatial Production Allocation Model) [23] and STARFM (Spatial and Temporal Adaptive Reflectance Fusion Model) [24]. According to the different principles of remote sensing spatio-temporal data fusion algorithms, the algorithms based on pixel reconstruction have been widely used in recent years. It is based on the idea of linear regression, which is simple in principle and calculation. Based on the idea of pixel reconstruction and moving window, STARFM was proposed in 2006. It makes full use of the spatial distance, spectral difference and time difference between target pixel and neighboring pixel, and greatly improves the fusion accuracy. Using this pair-based approach, subsequent scholars put forward many improved methods for Landsat and MODIS data fusion, such as Spatial Temporal Adaptive Algorithm for mapping Reflectance Change (STAARCH) [25] and Spatiotemporal Vegetation Index Image Fusion Model (STVIFM) [26]. Besides, researchers have fused Landsat, MODIS, Sentinel and other remote sensing image data, such as the NDVI downscaling methodology developed with images from the Sentinel-2A, Sentinel-2B, Landsat-7, and Landsat-8 orbital platforms [27]. In addition, the important research in this sense is the Enhanced Spatial and Temporal Adaptive Reflectance Fusion Model (ESTARFM), which comprehensively considers the temporal trend of reflectance change of the ground object and uses the spatial and spectral similarity of pixel to construct the central pixel [28]. By integrating the advantages of spatial distribution and quantitative expression of different data, crop planting structure extraction and agricultural information monitoring at national or global scales have been realized [29,30], such as M3 cropland datasets [31] and MIRCA-2000 (Monthly Irrigated and Rainfed Crop Areas Around the Year 2000) [32]. Therefore, great progress has been made in the study of remote sensing extraction of crops spatial patterns, which has played an important role in serving agricultural production, ensuring food security and promoting the study of global change.

At present, the number of crops types covered by the extraction of domestic crop planting structure was relatively small, and the research mainly concentrated on rice, wheat and maize, with less coverage of cash crops. Due to the short time span, most studies focused on static extraction at a single time point or period, which was difficult to be used to analyze the dynamic characteristics and rules. The study area was mainly northeast and north China, with simple cropping rotation patterns, rarely complex multi-cropping rotation areas. The study focused on relatively simple calculating the planting area of crops, but did not explore the dynamic characteristics of the spatial distribution and crop rotation patterns of various crops. As an important grain, cotton and oil production base in China, the Middle Yangtze Plain (MYP) is one of the most sensitive areas to the change of the coupling mechanism of the natural environment, economic development and agricultural production. The MYP has been greatly reduced in the cultivated area due to rapid urban expansion and massive urban construction and was the key area for

lost potential crops yield during this period [33,34]. Many serious issues have emerged during agricultural production; for example, long-term conservation tillage led to shallow and stringent ploughing layers [35]. Moreover, China's agricultural economic system and policies changed and reformed constantly in 1990–2020. Therefore, this study took the main crops (including rice, cotton, maize, soybean, winter wheat and rapeseed) in the MYP in 1990–2020 as the research objects, which had strong typicality and representativeness. Based on crop remote sensing extraction, we deeply explored the characteristics and driving factors of main crop spatio-temporal planting patterns change, which provided a scientific basis for sustainable agricultural development, assessment of the impact of policies on agriculture and protection of high-quality cultivated land.

The objectives of this study are to address the following three questions: how to map the planting spatial distribution of main crops with high accuracy considering crop rotation patterns and spectral and phenological characteristics in the MYP in 1990–2020? What are the characteristics of spatio-temporal patterns change of main crop planting at different stages? What are the main driving factors for spatio-temporal patterns change of main crop planting? In order to achieve these objectives, we, first, established the raster-based spectral and phenological differential change method (RSPDCM) based on Landsat and MODIS fusion data of long time series, extracted high-precision remote sensing information of rice, cotton, maize, soybean, rapeseed and winter wheat and then generated the spatio-temporal patterns data set of main crops in the MYP in 1990–2020. Second, we quantitatively analyzed the intensification, large-scale and agglomeration of main crop planting from the perspectives of the multi-cropping index, cropping systems, plot area and spatial autocorrelation. Finally, we selected six typical counties (or districts) to multi-angle explore the influencing mechanism of crop planting change in the MYP from the aspects of the physical geography, agricultural production and regional policy conditions. Combining the development trend of national agricultural production and the characteristics of regional agricultural production, we put forward reasonable suggestions for realizing sustainable agricultural development.

## 2. Data and Methods

### 2.1. Data

#### 2.1.1. Study Area

The MYP is located in the junction of Hunan, Hubei and Jiangxi provinces of China, belonging to the subtropical humid monsoon climate zone between 110°30'–117°30' E and 27°30'–32°00' N, including the Dongting Lake Plain (DTLP), Jiangnan Plain (JHP), Eastern Hubei Riverside Plain (EHRP) and Poyang Lake Plain (PYLP) (Figure 1). It has an administrative area of 10.55 million ha and 88 counties (or districts) under its jurisdiction, with a permanent population of 55.61 million in 2020 [7]. Cultivated land is the most important land-use type, accounting for more than 45% of the total land area, and water area accounts for more than 15%. The terrain in the MYP is low and flat, and the area below 50m above sea level accounts for 70.79% of the total land area. The mean annual precipitation is 1100–1800 mm. The mean annual average temperature is 15–18 °C. The accumulated temperature  $\geq 10$  °C is 4800–5800 °C. The MYP is a typical multi-cropping agricultural area [36], among which the PYLP, JHP and DTLP are the traditional high-yield commodity grain bases in southern China. Fifty-one counties (or districts) were listed as the top grain (or oil) producing counties (or districts) in 2020, accounting for 88.22% of the total land area [37].

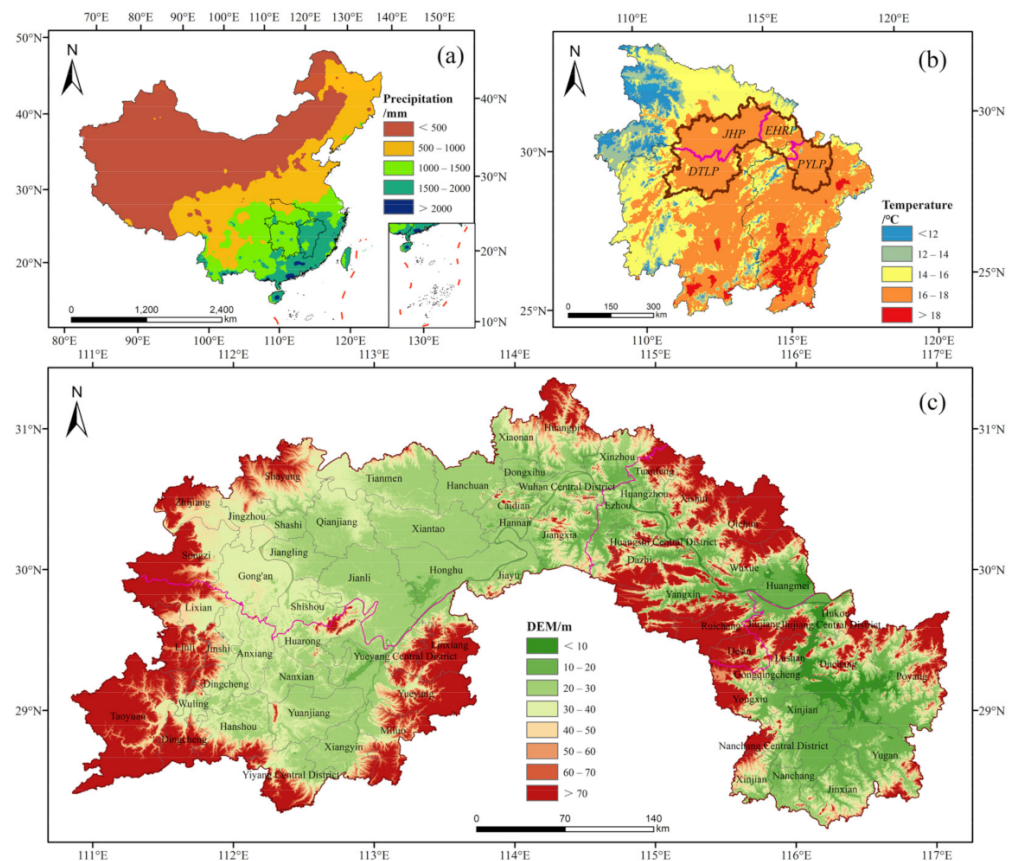


**Figure 1.** Location and physical geographical conditions of the MYP: (a) spatial distribution of annual mean precipitation and location of Hubei, Hunan and Jiangxi provinces in China; (b) spatial distribution of annual mean temperature in Hubei, Hunan and Jiangxi provinces and location of the MYP; and (c) spatial distribution of elevation in the MYP. (MYP: Middle Yangtze Plain, DTLP: Dongting Lake Plain, JHP: Jiangnan Plain, EHRP: Eastern Hubei Riverside Plain, PYLP: Poyang Lake Plain, similarly hereinafter).

### 2.1.2. Data Collection and Preprocessing

Landsat images from 1990 to 2020, with 30 m spatial resolution and 16d temporal resolution, were used in this study. The path/row number of Landsat images covering the MYP is 121/40, 122/39, 123/39, 123/40, 124/39 and 124/40. We preprocessed these data with radiometric calibration, atmospheric correction and vegetation index calculation. MODIS/Terra Vegetation Indices 16-Day L3 Global 250 m SIN Grid (MOD13Q1) products from 2000 to 2020, with 250 m spatial resolution, were used in this study. The path/row numbers of MOD13Q1 products are h27/v05, h27/v06, h28/v05 and h28/v06. We performed projection conversion, resampling, sub-data set extraction, clipping and so on for MODIS data. We obtained the algorithm code based on the ESTARFM from the website of CHENJIN\_LAB (<http://www.chen-lab.club/>, accessed on 15 July 2021). The accuracy of remote sensing classification results was verified by field investigation and visual interpretation of Google Earth high-resolution remote sensing images. The socio-economic data came from the China Rural Statistical Yearbook, Hunan Statistical Yearbook, Hubei Rural Statistical Yearbook, China County Statistical Yearbook and other county statistical yearbooks.

## 2.2. Methods

### 2.2.1. ESTARFM for Generating Landsat-MODIS Fusion Data

The research idea of data fusion using ESTARFM is that the high and low spatial resolution image pairs of the two corresponding time nodes close to the predicted time and



a low spatial resolution image of the simulated date were taken as the reference images. In addition, these five scenes were used as input data of ESTARFM to generate the fusion data at the predicted time, so as to obtain image data with a complete-time series.

Assuming that the predicted target pixel is a homogeneous single object type, ESTARFM ignores the atmospheric correction error and registration error, and only the sensor system deviation exists between Landsat image data and MODIS image data, where there is a linear relationship between their pixel reflectance.

$$H(x, y, t_p, B) = H(x, y, t_o, B) + a * (L(x, y, t_p, B) - L(x, y, t_o, B)) \quad (1)$$

where  $H(x, y, t_p, B)$  and  $H(x, y, t_o, B)$  are pixel values at  $(x, y)$  in  $B$  band of high spatial resolution remote sensing image at moments  $t_p$  and  $t_o$ , respectively.  $L(x, y, t_p, B)$  and  $L(x, y, t_o, B)$  are pixel values at  $(x, y)$  in  $B$  band of low spatial resolution remote sensing image at moments  $t_p$  and  $t_o$ , respectively.  $a$  is the model coefficient determined by the system deviation of the two image sensors.

As the above relation is not suitable for mixed pixels, to solve this problem, the ESTARFM model introduces the conversion coefficient and uses the pixels with high spectral similarity in the neighborhood as auxiliary information to calculate it. The specific idea is to set up a search window of a certain size centered on the predicted pixels, select the pixels that are similar to the predicted pixels, and convolve them with the weight function  $W$  to obtain the pixel value of the predicted pixels.

$$H(x_{w/2}, y_{w/2}, t_p, B) = H(x_{w/2}, y_{w/2}, t_o, B) + \sum_{i=1}^n W_i * V_i * (L(x_i, y_i, t_p, B) - L(x_i, y_i, t_o, B)) \quad (2)$$

where  $w$  is the size of the search moving window, which is mainly determined by the homogeneity of the ground object type.  $H(x_{w/2}, y_{w/2}, t_p, B)$  and  $H(x_{w/2}, y_{w/2}, t_o, B)$  are pixel values of the center pixel of the search window in the  $B$  band of high spatial resolution remote sensing image at moments  $t_p$  and  $t_o$ , respectively.  $n$  is the number of similar pixels including the central pixel.  $W_i$  is the weight of the  $i$  similar pixels, which determines the contribution of the  $i$  similar pixels to the reflectivity change of the central pixel. It is mainly determined by the spectral similarity of two images with different spatial resolutions at the similar pixel location and the distance between the similar pixel and the central pixel.  $V_i$  is the conversion coefficient of the  $i$  similar pixels.  $L(x_i, y_i, t_p, B)$  and  $L(x_i, y_i, t_o, B)$  are pixel values of the  $i$  similar pixels in the  $B$  band of low spatial resolution remote sensing image at moments  $t_p$  and  $t_o$ , respectively.

Then, the time weight  $T_k$  is calculated according to the change amplitude of pixel value of low spatial resolution image between time  $t_k$  and predicted time  $t_p$ .

$$T_k = \frac{1 / \left| \sum_{i=1}^n L(x_i, y_i, t_p, B) - \sum_{i=1}^n L(x_i, y_i, t_o, B) \right|}{\sum_{k=m,n} (1 / \left| \sum_{i=1}^n L(x_i, y_i, t_p, B) - \sum_{i=1}^n L(x_i, y_i, t_o, B) \right|)}, \quad k = m, n \quad (3)$$

To sum up, the following formula is the final calculation formula of the pixel value of the image at the predicted time  $t_p$  [28].

$$H(x_{w/2}, y_{w/2}, t_p, B) = T_m * H_m(x_{w/2}, y_{w/2}, t_p, B) + T_n * H_n(x_{w/2}, y_{w/2}, t_p, B) \quad (4)$$

where  $T_m$  and  $T_n$  are the time weights of fusion images calculated at moments  $t_m$  and  $t_n$ , respectively.  $H_m(x_{w/2}, y_{w/2}, t_p, B)$  and  $H_n(x_{w/2}, y_{w/2}, t_p, B)$  are the fused central pixel values calculated by Formula (2) at moments  $t_m$  and  $t_n$ , respectively.

In this study, using ESTARFM algorithm in ENVI-IDL module, the pre-processed different spatial resolution remote sensing images were spatio-temporal fused. High and low spatial resolution remote sensing images referred to Landsat and MODIS images,

respectively. Since Landsat images covering the MYP were often affected by cloud pollution, and the duration of the appropriate time windows for extracting various features was so short that it might be inundated by the low time resolution of the 16-day composites [15,38], we developed the Landsat-MODIS fusion data with 30 m spatial resolution. This study processed 476 Landsat-TM /OLI images and 207 MOD13Q1 images, with cloud cover of all data less than 50%, and produced about 90 Landsat-MODIS fusion images (Table S1).

Since Landsat images with different paths and row numbers were directly acquired on different dates, data fusion was conducted according to Landsat coverage. The Landsat image with path/row number 124/39 on 21 March 2020 was selected as an example (Figure 2). Landsat images of 31 January 2020 and 26 August 2020 and MODIS images of 2 February 2020 and 28 August 2020 were used as input image pairs, and the Landsat-MODIS fusion image with spatial resolution of 30 m was reconstructed according to the prediction of the MODIS image of 21 March 2020. Then, the Landsat-MODIS fusion image was compared with the Landsat image obtained on 19 March 2020. The size of the search moving window was set to 150 m  $\times$  150 m (5 pixels  $\times$  5 pixels). According to the fusion image, it can be found that the spatial resolution of the MODIS image can be improved from 250 m to 30 m using the ESTARFM model, which is basically consistent with the real Landsat image. Meanwhile, the cloud covered area on Landsat image can be clearly restored. Through visual observation, it can be found that the original pixel value is basically retained. In the fusion image and comparison image, 3266 points were randomly selected for correlation analysis in areas without cloud cover (Figures S1 and S2), and the correlation coefficients were 0.9049 and 0.8749 of NDVI and EVI. Therefore, the fusion image processed by the ESTARFM model can be used for crop extraction in the MYP.

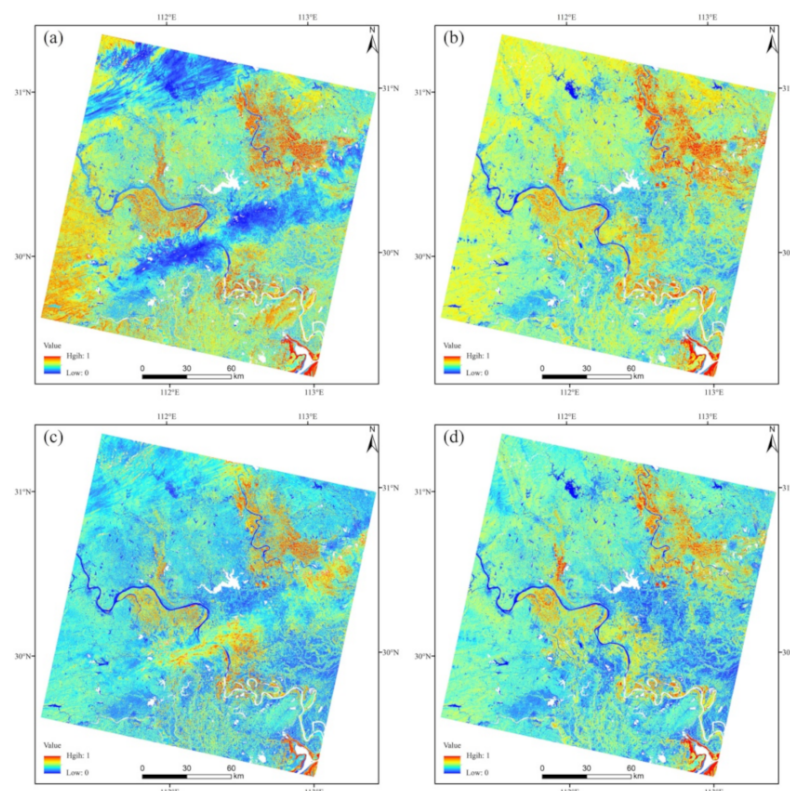


**Figure 2.** Comparison of original Landsat data and Landsat-MODIS fusion data: (a) NDVI values of the original Landsat image with path/row number 124/39 on 21 March 2020, (b) NDVI values of the Landsat-MODIS fusion data of the Landsat image with path/row number 124/39 on 21 March 2020, (c) EVI values of the original Landsat image with path/row number 124/39 on 21 March 2020 and (d) EVI values of the Landsat-MODIS fusion data of the Landsat image with path/row number 124/39 on 21 March 2020.

### 2.2.2. Construction of Vegetation Index Curves of Main Crops

The summer and autumn crops planted in the MYP are single rice, double-cropping rice (early rice and late rice), cotton, maize and soybean, and the overwintering crops are winter wheat and rapeseed (Figure 3). Single rice, whose growth period is 130–150 days, is sowed in late April and early May, transplanted in mid-June and harvested in late September and early October. Early rice, whose growth period is 105–115 days, is sowed in late March, transplanted before 30 April, and harvested in late July. Late rice, whose growth period is 115–120 days, is sowed before mid-June, transplanted in mid-July and harvested in mid-late October. Spring maize, whose growth period is 110–120 days, is sowed around 20 March and harvested around 20 July. Spring soybean, whose growth period is 90–100 days, is sowed in early April and harvested in mid- to late-July. Summer maize and soybean, whose growth period is 95–110 days, is sowed in early June and harvested in early October. The planting methods of cotton include two ways: transplanting after seedling raising with nutrition bowl and sowing directly after wheat (or rapeseed) harvesting. In the first way, cotton grows for 120–130 days, being sowed around 20 April on sunny days and transplanted around 20 May. In the second way, cotton grows for about 100 days, directly being sowed in late May to early June in the field and by 10 June at the latest. Cotton harvest lasts longer, generally from mid-September to mid-October. Rapeseed is grown in a similar way to cotton. The growth period of rapeseed transplanted after sowing is 180 to 240 days. Rapeseed is sown in mid- to late-September and transplanted at about 30 days of seedling age. However, rapeseed sown directly without transplanting has a growth period of 160–210 days, being sowed in late October, flowering in March of the following year and harvested in April of the following year. Wheat has a growth period of 220–240 days, is sowed from late October to early November, with the best sowing period from 24 to 31 October, and is harvested in May of the following year. In summary, the main crop rotation patterns in the MYP are double-cropping rice, double-cropping rice and overwintering crops, single rice, single rice and overwintering crops, maize, maize and overwintering crops, soybean, soybean and overwintering crops, cotton and cotton and overwintering crops.

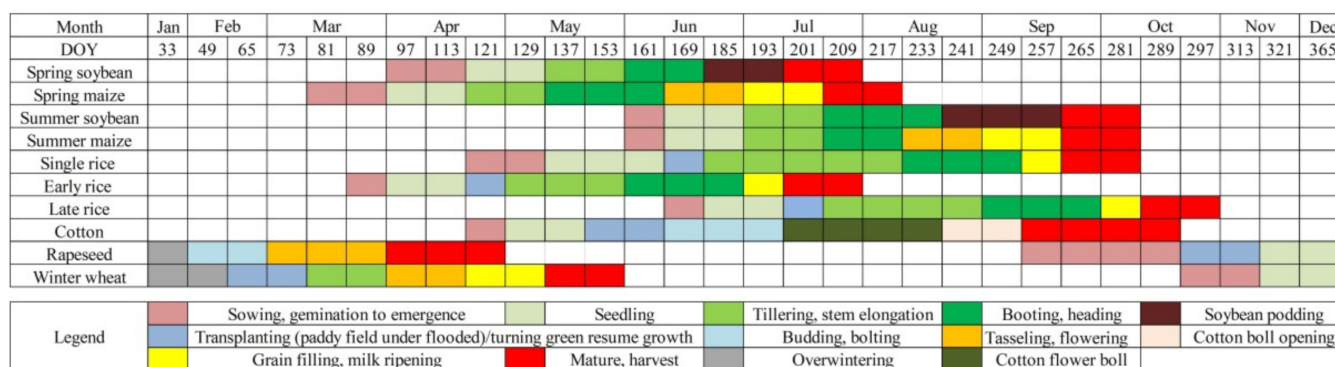


**Figure 3.** Phenological calendar of main crops in the MYP: Day of Year (DOY) represents the end time of the phenological period. Due to the temporary sudden weather change or the planting time arrangement of individual farmers, the planting phenology of certain crops in some areas might be advanced or delayed by up to 5 days.

In different phenological periods, there were significant differences in remote sensing images and vegetation index of different crops, which provided the theoretical premise for the extraction of spatial distribution patterns of the main crops. We used 1651 samples to obtain the reflectance of thirteen land-cover types: woodland, construction land, bare land, grassland, water body, cultivated land, single rice, double-cropping rice, cotton, soybean, maize, rapeseed and winter wheat, with 127 sample points for each type (Figure 4). The sampling method is to select the areas where a certain crop has been planted continuously

from 1990 to 2020 through visual interpretation and field survey. In addition, we calculated vegetation index mode for typical features in different phenological periods (Figure 5).

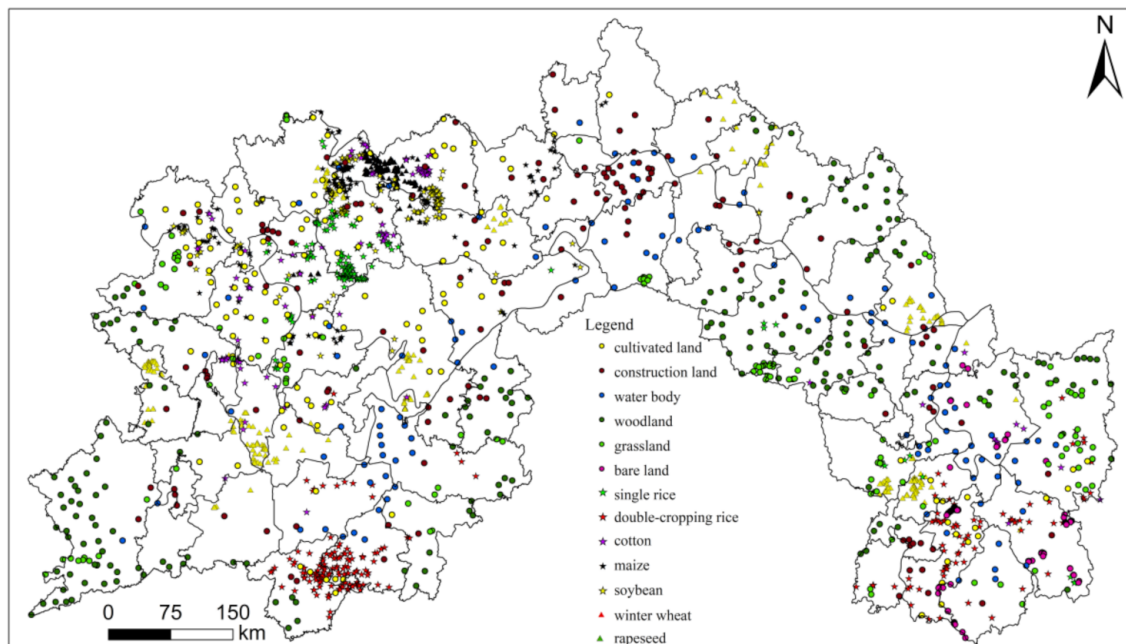


**Figure 4.** Distribution map of sample points for construction of crop vegetation index curves in the MYP.

### 2.2.3. RSPDCM for Main Crop Planting Extraction

In this study, based on long time series Landsat-MODIS fusion data, we developed a RSPDCM to combine crop rotation patterns with dynamic changes of vegetation index curves.

Firstly, we extracted first-level land-use types, including woodland, construction land, bare land, grassland, water body and cultivated land. June to September was the proper time window to distinguish water body, construction land and bare land. At this period, all kinds of vegetation grew vigorously and the area with low NDVI [39] and EVI [40] values was water body or construction land, meanwhile the area with high MNDWI [41] value or no EVI value was water body. November–January was an important time window for identifying woodland and grassland. At this time, the summer and autumn crops were not sown, and the overwintering crops were in the overwintering or seedling stage, so the green vegetation with the highest NDVI and EVI values are woodland and grassland.

Secondly, we used EVI curves variation differences to extract overwintering crops. The appropriate period to extract rapeseed and winter wheat areas was between mid-March and early April. In this period, rapeseed and winter wheat showed different colors on true-color satellite images that rapeseed at flowering was yellow, and winter wheat at booting and heading was dark green.

Thirdly, we used the time window of irrigated field or rice transplanting period to extract paddy field and dryland. Late April, mid-June and mid- to late-July were the periods of paddy fields soaking or transplanting early rice, single rice and late rice.



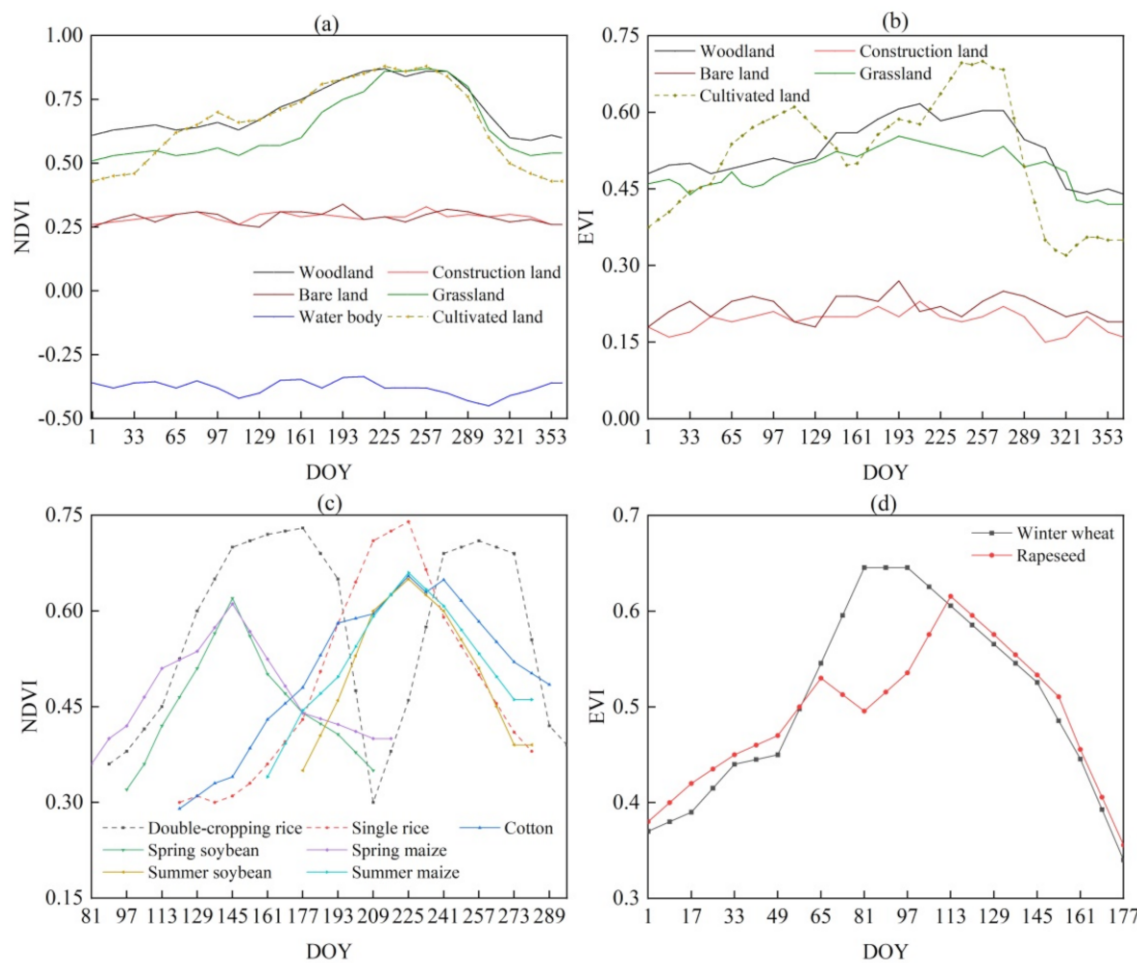


**Figure 5.** Vegetation index change curves of typical features in the MYP: (a,b) are the NDVI and EVI change curves of first-level land-use types; (c) is the NDVI change curves of summer and autumn crops; and (d) is the EVI change curves of overwintering crops.

Fourthly, we used NDVI curves differences to extract various summer and autumn crops. From early May to mid-August, the NDVI curves of the plots planted with single rice were unimodal, while those of double-cropping rice were bimodal [15]. Mid-June to early July was the window to distinguish cotton from other dryland crops. At this time, cotton was in the budding and bolting stage, during which cotton plants grew fastest with a higher NDVI value. Spring soybean and maize were in podding stage, tasseling or milk ripening stage, while summer soybean and maize were in the seedling, tillering and stem elongation stages, during which the NDVI value was lower. Mid-July to early August and mid-August to late September were good windows for distinguishing maize from soybeans. There were differences among varieties of maize and soybean for the vegetation index during the growing season [42], and the NDVI value of maize was higher at those times.

Finally, according to crop rotation patterns, we manually corrected the preliminary extraction results of main crop planting. Different summer and autumn crops or overwintering crops were spatially independent of each other in the year; for example, a plot of cultivated land already planted with winter wheat could not be planted with rapeseed. Furthermore, a plot planted with overwintering crops also were planted with summer and autumn crops in the same year. The main steps of extracting typical features of the MYP were summarized in Figure 6.

The statistical data of various crops in the MYP were sorted out and compared with the remote sensing identification results to calculate the relative errors (Table 1). The relative errors between the remote sensing extraction data and statistical data of main crops in the

MYP from 1990 to 2020 were all less than 20%. Verification samples are used to verify the classification results (Figures S1 and S2), and the accuracy results of the confusion matrix are shown in Table 2. The classification results of main crops in the MYP were quantitatively analyzed by classification confusion matrix, with the overall classification accuracy being higher than 89%, and the Kappa coefficient was higher than 0.8. Compared with other years, the planting area of main crops in 1990 and 2005 was lower, and the average plot area in 2015 and 2020 was smaller and more dispersed. Therefore, the low planting area of crops, the fragmentation of cultivated land and the presence of mixed pixels led to the low accuracy of these years.

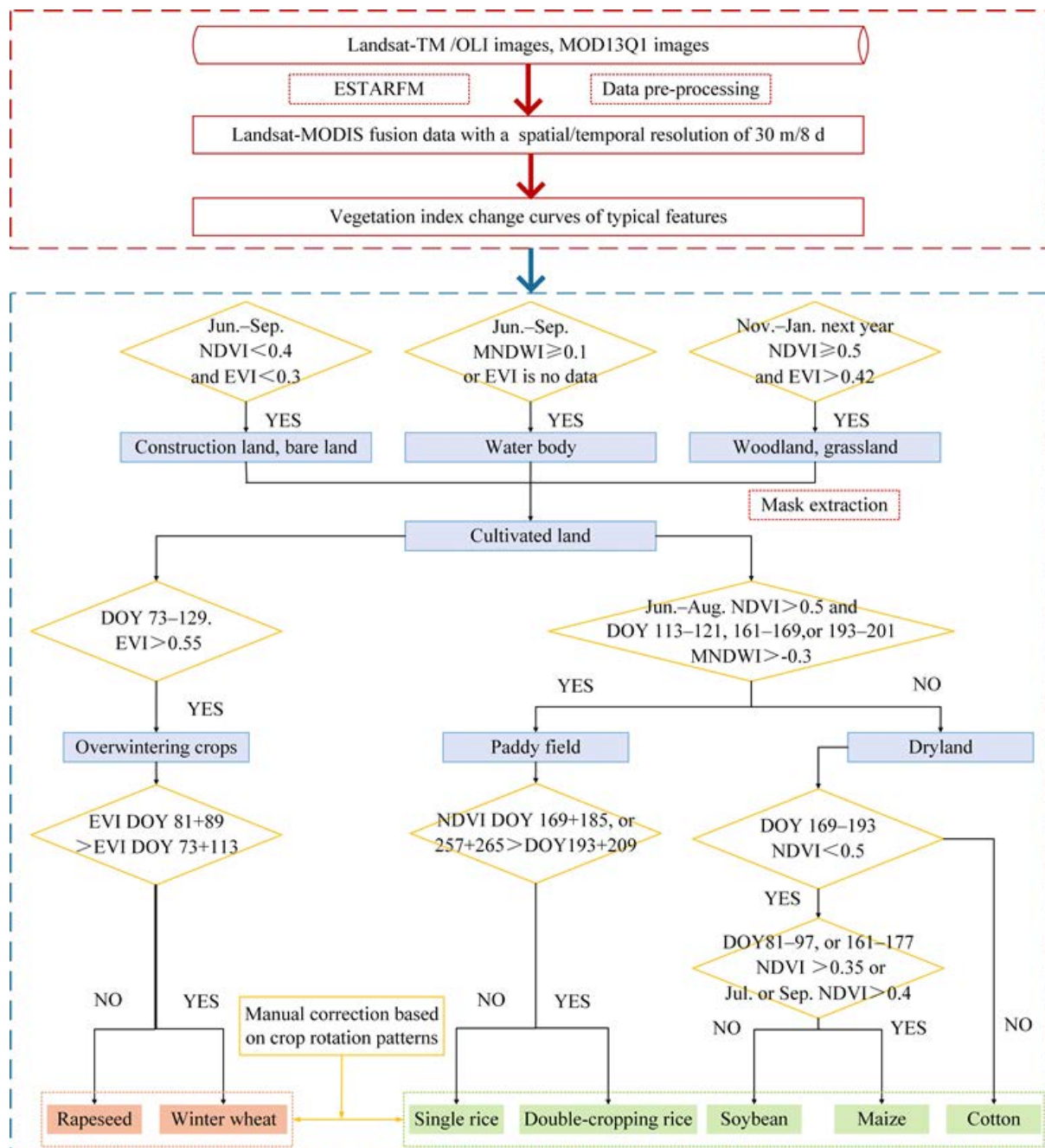


**Figure 6.** Technical route of the RSPDCM. The figure reflected the basic idea of extracting the spatial distribution of main crops. Due to remote sensing images quality and other aspects, individual thresholds were slightly adjusted.

**Table 1.** Accuracy assessment of main crop spatial distribution maps in 1990–2020 in comparison with statistical data.

Types		1995	2000	2005	2010	2015	2020
Cultivated land	SA	3.51	3.36	3.29	3.17	3.25	2.85
	RE	−5.70	−12.60	−14.56	−6.45	−11.12	−17.13
Single rice	SA	1.08	1.36	1.10	1.74	1.33	1.20
	RE	−15.58	−14.21	16.43	−11.35	−16.05	−11.63
Double-cropping rice	SA	2.77	1.41	1.39	1.21	2.02	1.17
	RE	17.58	16.05	−14.81	−13.31	−15.35	−14.55
Cotton	SA	0.37	0.57	0.37	0.46	0.28	0.22
	RE	−13.39	−11.43	11.05	−10.86	−16.53	−24.52
Maize	SA	0.22	0.20	0.16	0.27	0.39	0.38
	RE	14.69	12.55	18.51	15.33	13.85	15.50
Soybean	SA	0.17	0.20	0.30	0.15	0.18	0.17
	RE	20.02	12.41	16.59	18.56	19.36	16.94
Winter wheat	SA	0.32	0.35	0.38	0.47	0.42	0.30
	RE	12.50	17.44	13.08	12.56	−10.65	−11.39
Rapeseed	SA	0.88	0.79	0.58	0.76	1.20	0.73
	RE	5.05	5.37	7.57	12.71	−15.77	−16.95
Mean value		4.39	3.20	6.73	2.15	−7.56	−8.63

SA is the statistical area and its unit is millions of hectares. RE is the relative error and is expressed as a percentage. Double-cropping rice planting area is the sum of early rice and late rice planting areas. Due to problems in obtaining statistical data, this table did not include the statistical data of the MYP in 1990 and Yugan County and Poyang County in Jiangxi Province from 1990 to 2020.

**Table 2.** Accuracy assessment of main crop spatial distribution maps in 1990–2020 in comparison with validation samples.

Year	1990	1995	2000	2005	2010	2015	2020
Overall accuracy /%	89.6	93.4	94.3	93.1	93.6	94.1	93.8
Kappa coefficient	0.81	0.86	0.87	0.86	0.86	0.87	0.86
Producer's accuracy /%	82.3	86.5	89	86.1	87.1	87.5	87.2
User's accuracy /%	93.5	96.5	98.5	96.8	97.3	98.1	97.5
Sample numbers	13,506	14,003	13,956	14,102	13,821	13,987	14,222

The accuracy evaluation results in this table are the mean values of the accuracy evaluation results of cultivated land, rice, cotton, maize, soybean, winter wheat and rapeseed in a year.

#### 2.2.4. Spatio-Temporal Patterns Change Characteristics of Main Crop Planting

The spatio-temporal dynamics characteristics of main crop planting were analyzed in terms of the overall spatial distribution, intensification, scale and agglomeration characteristics in 1990–2020. We first compared the main crop distribution planting maps for individual years to determine the change trends in their spatial distribution at different stages.

$$\text{Area proportion}_k = \text{Area}_k / \text{Area}_{\text{total}} * 100\% \quad (5)$$

$$\text{Annual area change rate} = (\text{Area}_i - \text{Area}_j) / \text{Area}_i * 100\% \quad (6)$$

$$\text{Variable dynamic attitude} = (\text{Area}_{\text{in}} - \text{Area}_{\text{out}}) / (\text{Area}_{\text{in}} + \text{Area}_{\text{out}}) * 100\% \quad (7)$$

where  $k$  represents different kinds of crops, including rice, cotton, maize, soybean, winter wheat and rapeseed.  $\text{total}$  represents the whole main crops.  $i$  and  $j$  represent different years, including 1995, 2000, 2005, 2010, 2015 and 2020.  $\text{in}$  represents other land-use types transferred to this calculation type, while  $\text{out}$  is opposite.

Main crop intensification planting was primarily the production of two or more crops per year on the same plot of land, manifested in the narrowing of the exploitable gap between average actual planting area and genetic planting area potential [43]. In this study,

the measurement indexes of characteristics of main crop intensive planting were cropping system (including single, double and triple cropping per year) and multi-cropping index.

$$\text{Cropping index} = \frac{\text{Area}_{\text{single}} + 2 * \text{Area}_{\text{double}} + 3 * \text{Area}_{\text{triple}}}{\text{Area}_{\text{single}} + \text{Area}_{\text{double}} + \text{Area}_{\text{triple}}} * 100\% \quad (8)$$

where  $\text{Area}_{\text{single}}$ ,  $\text{Area}_{\text{double}}$  and  $\text{Area}_{\text{triple}}$  represent the areas of single, double and triple cropping per year and the cultivated area where main crops are grown, respectively.

The large-scale use of cultivated land is contrary to the fragmentation of cultivated land. From 2009 to 2018, about 73% of China's land plots area reached more than 3.33 ha, and the median land plots circulation area reached 13.33 ha [44]. We assumed that vector surface size was the area of each plot according to the results of raster data extraction of main crop planting. Considering regional crop-planting differences, the maximum plot area, the average plot area, the total area of a plot exceeding 10 ha and its proportion of main crop planting area were selected to reflect the scale of crop planting.

Finally, in order to reveal the spatial agglomeration characteristics of main crops in the MYP, we used Global Moran's I index to distinguish the Global spatial autocorrelation of main crops in different townships, and revealed the clustering characteristics of local spatial distribution by the Hot Spot Analysis method [45].

$$I = \frac{n \sum_{i=1}^n \sum_{j=1}^n w_{i,j} z_i z_j}{(\sum_{i=1}^n \sum_{j=1}^n w_{i,j}) \sum_{i=1}^n z_i^2} \quad (9)$$

$$G_i^* = \frac{\sum_{j=1}^n w_{i,j} x_j - \bar{X} \sum_{j=1}^n w_{i,j}}{\sqrt{\frac{\sum_{j=1}^n x_j^2}{n} - (\bar{X})^2} \sqrt{\frac{[n \sum_{j=1}^n w_{i,j}^2 - (\sum_{j=1}^n w_{i,j})^2]}{n-1}}} \quad (10)$$

$$\bar{X} = \frac{\sum_{j=1}^n x_j}{n} \quad (11)$$

where  $x_i$  and  $x_j$  are attribute values for features  $i$  and  $j$ .  $z_i$  and  $z_j$  are the deviation of an attribute for feature  $i$  and  $j$  from their mean ( $x_i - \bar{X}$  and  $x_j - \bar{X}$ ).  $w_{i,j}$  is the spatial weight between features  $i$  and  $j$ .  $n$  is equal to the total number of features.  $I$  is the Global Moran's I index.  $G_i^*$  is the Getis-Ord  $G_i^*$  statistic.

### 3. Results

#### 3.1. Main Crop Distribution Mapping

From 1990 to 2020, the spatio-temporal patterns of main crop planting in the MYP have changed frequently, with the average annual planting area of 5.14 million ha and the average annual cultivated area of main crops of 2.94 million ha (Figure 7). Rice was the largest crop in the MYP, with an annual planting area of 3.04 million ha and an area proportion of 58.3% (Figure 8). Rapeseed followed with 0.84 million ha, accounting for 16.45% (Figure 9). The annual planting area of cotton, maize and soybean was about 0.35 million ha, accounting for about 6.5%. The winter wheat planting area was the smallest, with an annual planting area of 0.22 million ha, accounting for 4.45%.



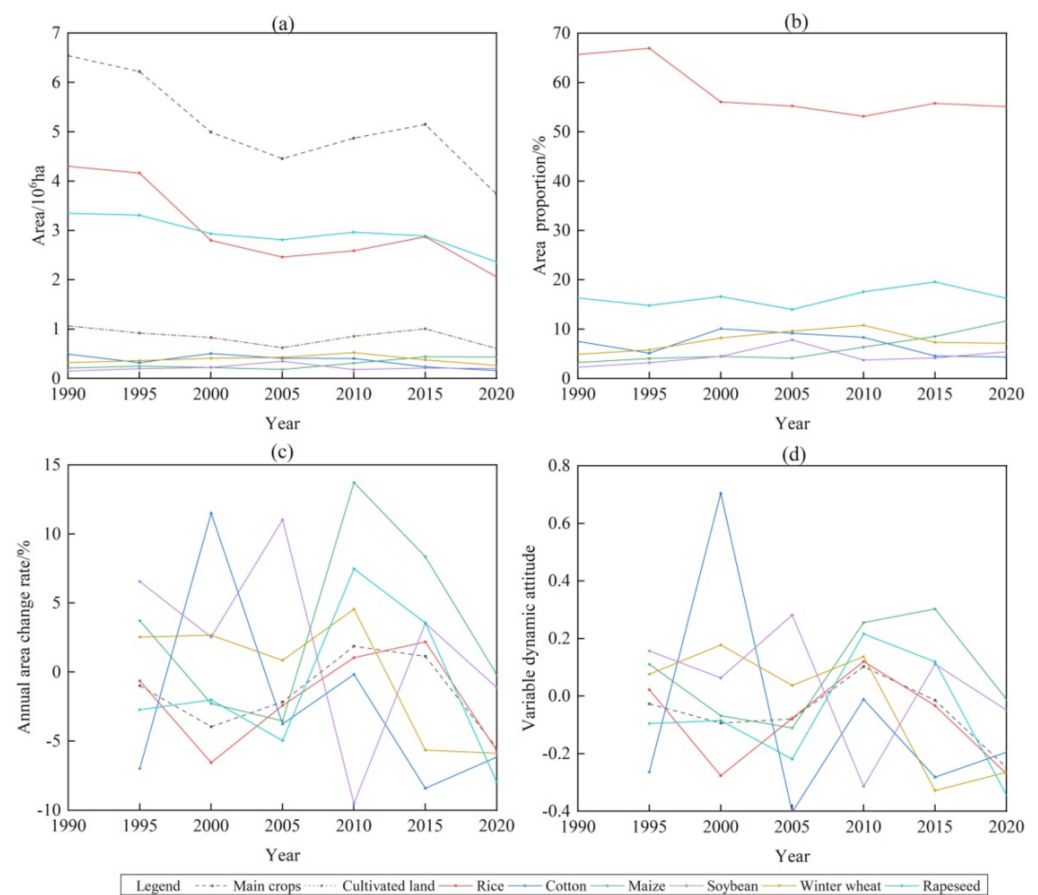


**Figure 7.** Main crop planting condition in the MYP in 1990–2020: (a) the planting area and the area of cultivated land for main crops; (b) area proportion of main crop planting; (c) annual area change rate of main crop planting; and (d) variable dynamic attitude of main crop planting.

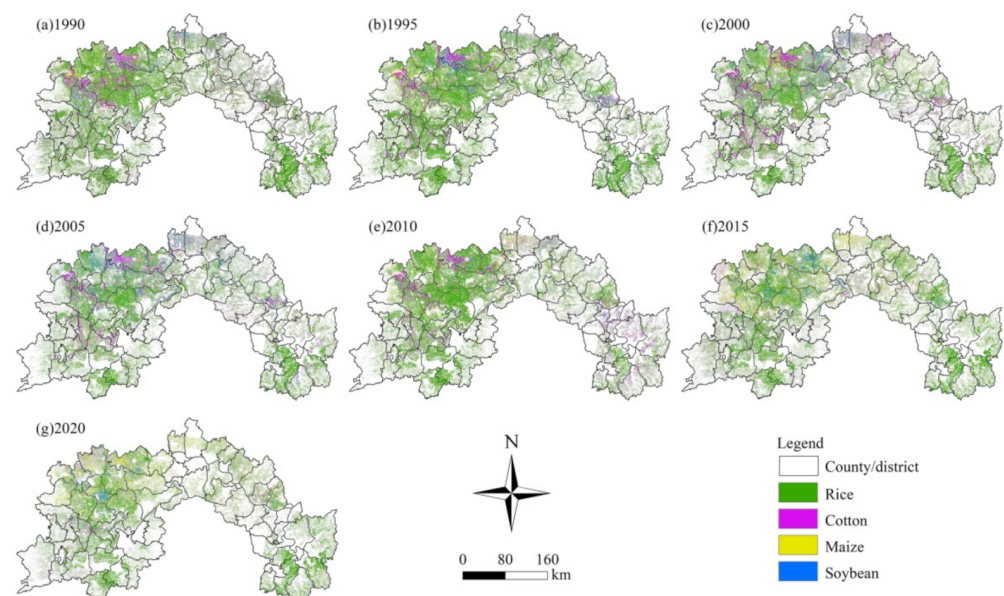


**Figure 8.** Spatial distribution of summer and autumn crop planting in the MYP in 1990–2020. Figure (a–g) represent the spatial distribution of rice, cotton, maize and soybean in the MYP in 1990, 1995, 2000, 2005, 2010, 2015 and 2020, respectively.

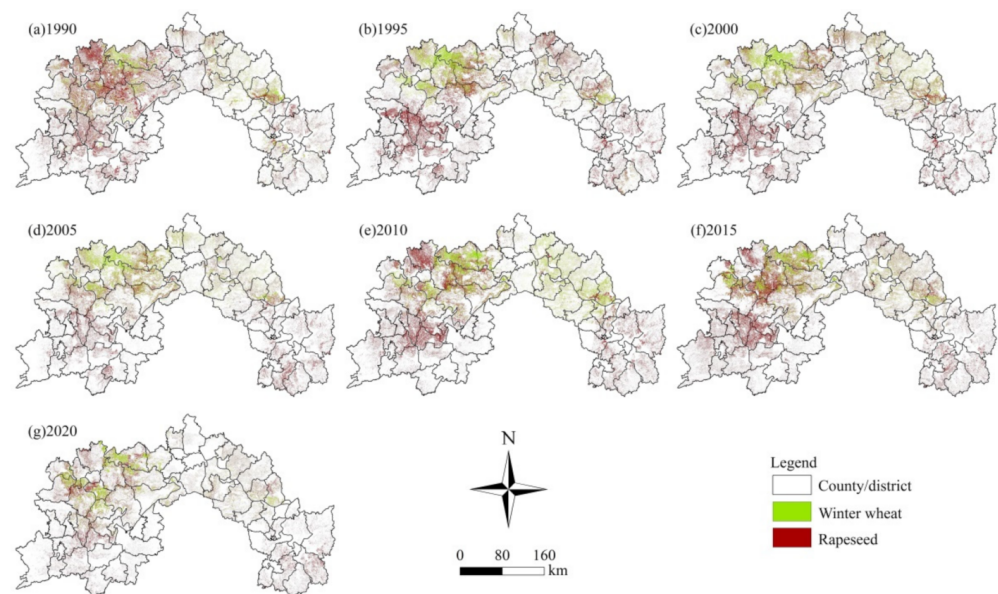


**Figure 9.** Spatial distribution of overwintering crop planting in the MYP in 1990–2020. Figure (a–g) represent the spatial distribution of winter wheat and rapeseed in the MYP in 1990, 1995, 2000, 2005, 2010, 2015 and 2020, respectively.

During the past 30 years, the planting area of main crops in the MYP showed a trend of fluctuation and decline, with the planting area decreasing from 6.54 million ha to 3.73 million ha and an annual decrease of 93,696 ha. The change of trend of cultivated area and the total planting area of main crops was basically consistent, but cultivated area fluctuated less, with an average annual decrease of 33,083 ha. The overall change of planting area of main crops was divided into three stages: 1990–2005, 2005–2015 and 2015–2020, respectively. The planting area of main crops in the MYP was in a continuous transition state in 1990–2005 and 2015–2020. The planting structure of crops was constantly adjusted, which the area proportion of rice and rapeseed was constantly decreasing and of winter wheat and soybean was greatly increasing. The planting area of main crops in the MYP rose briefly in 2005–2015. From 1990 to 2020, rice, cotton and rapeseed were the crops with decreasing planting area and area proportion, with the annual area decrease of 74,728 ha, 10,981 ha and 15,353 ha and the area proportion of 10.58%, 3.16% and 0.05%, respectively. The planting changes of winter wheat were characterized by a rapid decrease in the area, but a slight increase in the area proportion, with an annual area decrease of 1836 ha and the area proportion increase of 2.22%. Maize and soybean were the crops with increasing planting area and its proportion, with the annual planting area of 7438 ha and 1762 ha and the area proportion of 8.42% and 3.14%, respectively.

In conclusion, the main crop planting area in the MYP fluctuated significantly in 1990–2020, during which the change of rice and rapeseed planting area basically determined a total variation trend. However, due to the area proportion decrease in rice and rapeseed, winter wheat, maize and soybean tended to have significant substituting effects. Cotton, as a cash crop with great fluctuation in market price, was an important time point for its change in 2010, and its area decreased by nearly 60% in the past 10 years. In addition, the decrease difference between planting area and cultivated area of main crops reflects the important impact of main crop intensification planting on agricultural production in the MYP.

### 3.2. Characteristics of Main Crop Intensification Planting

From 1990 to 2020, the cropping intensification of main crops in the MYP showed a trend of fluctuating decline, and the multi-cropping index decreased from 195.37% to 158.23%, with an average annual decline of 1.24% (Figure 10). The multi-cropping index

and area decreased rapidly in 1990–2005 and 2015–2020. The lowest area proportion of double and triple cropping per year was 46.10% (2005) and 0.38% (2020), respectively. From 2005 to 2015, the multi-cropping index and area briefly increased, the area proportion of single cropping per year decreased to 14.81% and the area proportion of double cropping per year increased to 72.54%. In the past 30 years, the cropping system changed from mainly double cropping per year to single cropping per year.

From 1990 to 2005, the multi-cropping index of cultivated land among townships in the MYP decreased rapidly, with a big difference. The annual average of the multi-cropping index was 175–250% in the PYLP and DTLP, 150–225% in the EHRP and 100–200% in the JHP. From 2005 to 2015, the change of trend of the multi-cropping index of cultivated land among townships was different. Most townships in the DTLP, PYLP and JHP showed an upward trend, while the multi-cropping index of cultivated land in the urban center showed an obvious downward trend. From 2015 to 2020, the multi-cropping index of cultivated land among most townships of the MYP decreased by 5–50% compared with the previous period, and the number of townships with the multi-cropping index over 200% was further reduced. From 1990 to 2020, the high values of cropland multi-cropping index were mainly in Xiangyin, Yuanjiang, Hanshou and Yueyang counties (districts) of the south of the DTLP, Nanchang, Xinjian, Nanchan, Jinxian and Duchang counties (districts) of the PYLP and Wuxue city in the EHRP, while the low values were mainly in the urban center (Figure 11). In conclusion, in the past 30 years, the intensification degree of main crops in the PYLP was characterized by high intensity and small decrease, while that in the JHP and EHRP was low intensity and large decrease and that in the DTLP was high intensity and large decrease.

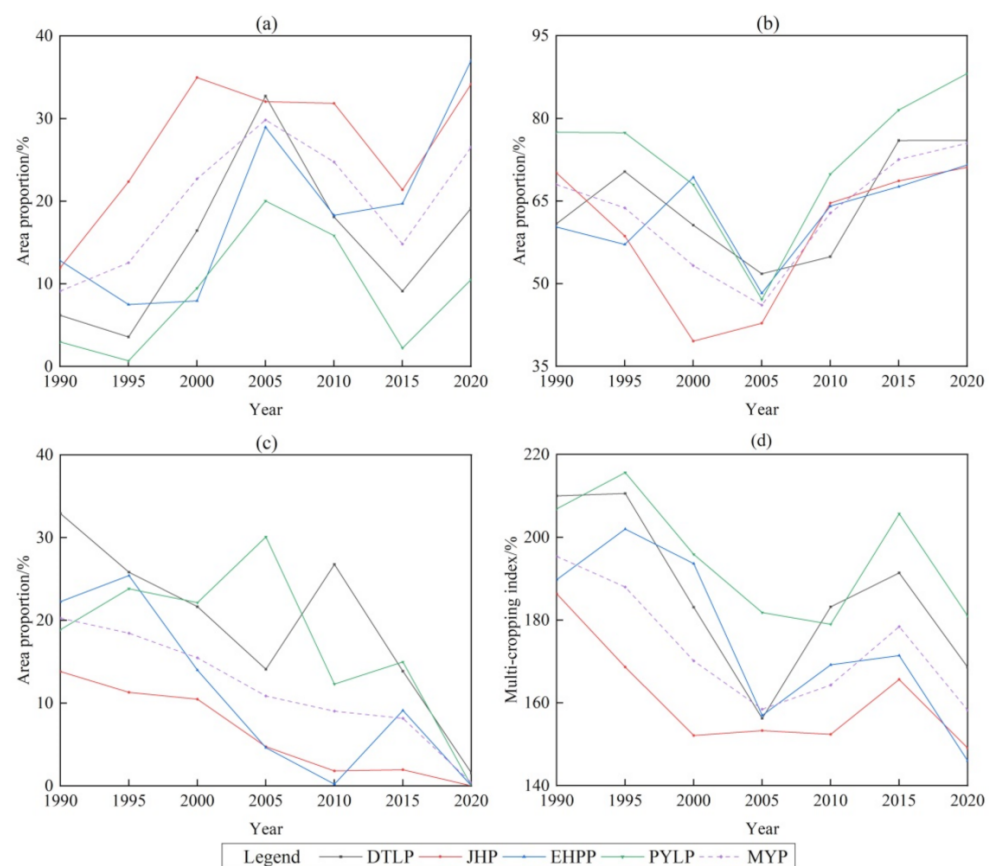


**Figure 10.** Changes of main crop intensification planting in the MYP in 1990–2020: (a–c) are the area proportion of cultivated land with single, double and triple cropping per year, respectively; (d) is the multi-cropping index of cultivated land.

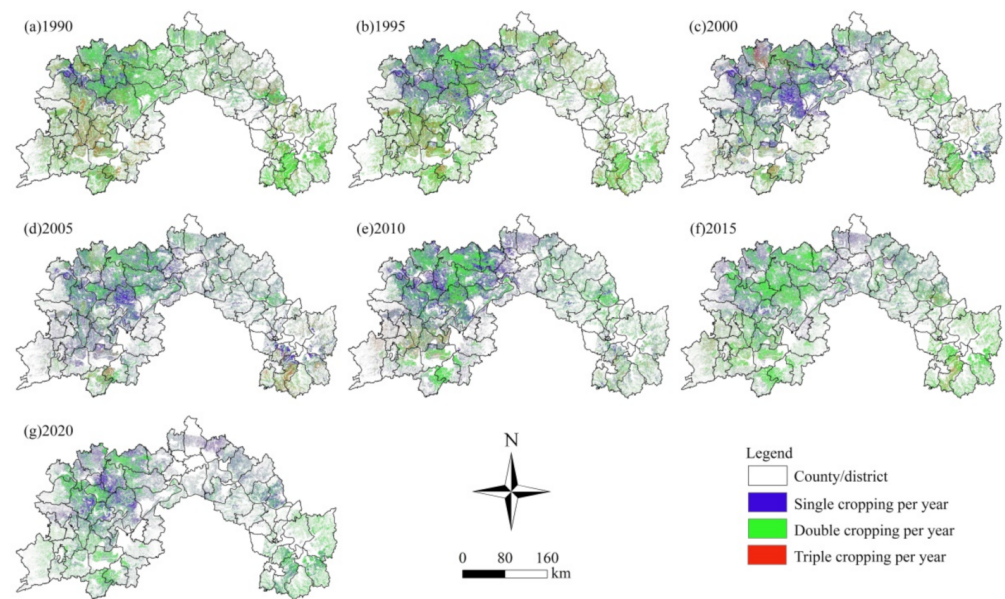


**Figure 11.** Spatial distribution of main crop intensification planting in the MYP in 1990–2020. Figure (a–g) represent the spatial distribution of single cropping per year, double cropping per year and triple cropping per year in the MYP in 1990, 1995, 2000, 2005, 2010, 2015 and 2020, respectively.

### 3.3. Characteristics of Main Crop Large-Scale Planting

China has traditionally adopted labor-intensive cultivation practices with small land areas, high costs and low labor productivity, which has utilized labor-intensive cultivation practices compared to developed countries [46]. From 1990 to 2020, the large-scale cultivation of main crops in the MYP showed a state of polarization (Figure 12). On the one hand, the fragmentation degree of decentralized cultivation plots of each household increased; on the other hand, the number and area of plots operated by new farmer cooperative organizations and large enterprises increased significantly. We found rice was the best crop species in large-scale cultivation in the MYP, with an average plot area of 1.05 ha and a maximum plot area of 27,467 ha, and a plot area over 10 ha accounted for 29.29% of the total rice planting area from 1990 to 2020. Rapeseed and winter wheat followed, with an average annual area of 0.48 ha and 0.49 ha, the maximum area of 7242 ha and 4003 ha and plot area over 10 ha accounting for 22.09% and 41.68%, respectively. Cotton, maize and soybean were the worst crop species in large-scale cultivation, with an average annual plot area of about 0.2 ha, a maximum plot area of about 800 ha and a plot area over 10 ha accounted for about 13%. In the past 30 years, the degree of fragmentation of cultivated land for rice and cotton increased by a large margin, rapeseed, maize and soybean decreased and winter wheat changed little. From the analysis of spatial distribution, the plots with the largest areas of rice and rapeseed are mainly distributed in Nanchang and Jianli counties of the PYLP, Yuanjiang and Anxiang counties of the DTLP and so on, while the plots with the largest areas of cotton, winter wheat, maize and soybean are mainly distributed in Jingzhou Center District, Tianmen City, Wuxue City, Jiangling County and so on.



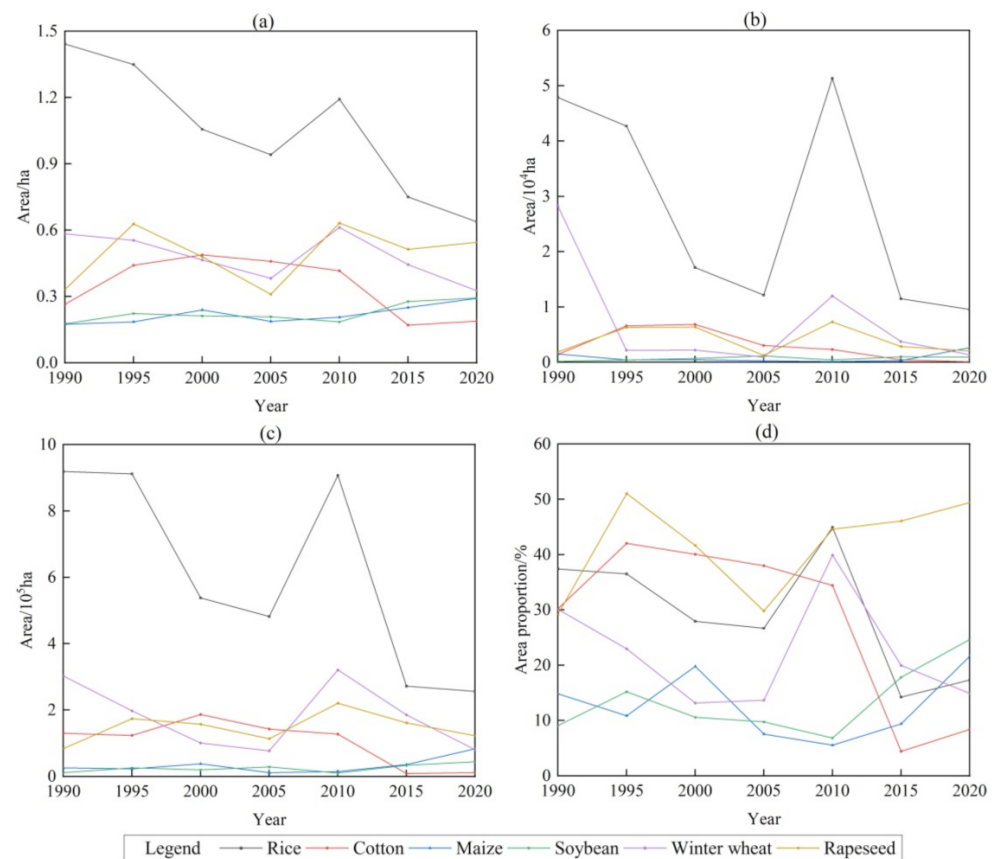


**Figure 12.** Situation of main crop intensification planting in the MYP in 1990–2020: (a) is the average plot area of main crop planting; (b) is the maximum plot area of main crop planting; (c,d) are the total area of a plot exceeding 10 ha and its proportion of main crops.

### 3.4. Characteristics of Main Crop Agglomeration Planting

We analyzed the overall agglomeration of the spatio-temporal patterns of main crop area (Table 3). The spatial distribution of the main crops in the MYP showed a very significant positive spatial aggregation, which was not random. With the development of time, the spatio-temporal patterns of the main crops were consistent with the change of trend of planting area. The positive spatial aggregation of rice was the most significant, followed by rapeseed and cotton, and maize, soybean and winter wheat were the worst. Local autocorrelation showed that the high-yielding areas of rice and rapeseed were concentrated in the JHP, the central DTLP and the southwest PYLP as well as a small amount in the central EHRP (Figure 13). The hot spots of maize, soybean and winter wheat are concentrated in the JHP and Wuxue City of the EHRP. The low-yield townships of crops gathered in the urban center, and their spatial distribution was stable and their range was obviously expanded. During the past 30 years, the planting area of rice and rapeseed hot spots decreased in the JHP, but increased in the PYLP and EHHP. The planting area of cotton, maize, soybean and winter wheat hot spots mainly occurred around Jingzhou City and Wuhan City.

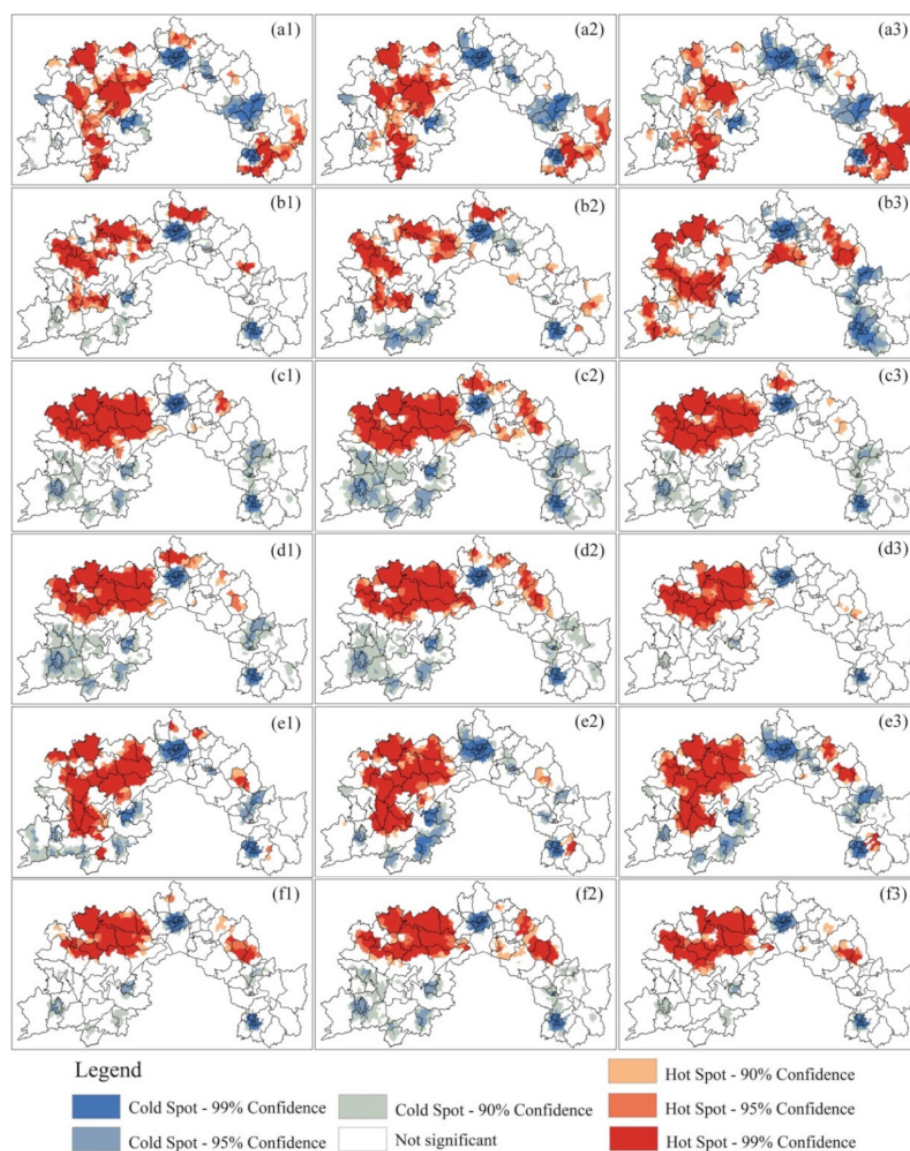


**Figure 13.** Getis-Ord Gi statistic of main crops area among townships in the MYP in 1990–2020: (a1)–(f1) are the hot spot analysis results of rice, cotton, maize, soybean, winter wheat and rapeseed in 1990–2005, respectively; (a2)–(f2) are the hot spot analysis results of rice, cotton, maize, soybean, winter wheat and rapeseed in 2005–2015, respectively; (a3)–(f3) are the hot spot analysis results of rice, cotton, maize, soybean, winter wheat and rapeseed in 2015–2020, respectively.

**Table 3.** Global Moran’s I index of main crop area among townships in the MYP in 1990–2020.

Year	Main Crops	Rice	Cotton	Maize	Soybean	Winter Wheat	Rapeseed
1990	0.577	0.5653	0.3179	0.215	0.2409	0.2997	0.3494
1995	0.6017	0.5636	0.2285	0.2753	0.2434	0.2189	0.4898
2000	0.5514	0.469	0.3028	0.2199	0.2755	0.2297	0.4902
2005	0.5285	0.4739	0.284	0.2835	0.2813	0.2474	0.41
2010	0.5289	0.4451	0.2883	0.3138	0.2839	0.2947	0.3531
2015	0.5717	0.5049	0.3874	0.2856	0.2392	0.2516	0.4256
2020	0.5116	0.4619	0.3081	0.2575	0.2031	0.1895	0.3903

The Z value of Global Moran’s I in the table is much higher than 2.58, and the P value is much less than 0.01, which has passed the significance test at the 1% level.

## 4. Discussion

### 4.1. Main Crop Planting Situation in Typical Counties

In order to explore the regional differences in the spatio-temporal patterns of the main crops in the MYP, we selected six counties to analyze the driving factors in typical regions, namely, Jianli City, Xiantao City, Nanchang County, Poyang County, Dingcheng District and Qichun County (Figure 1). Among them, under the background of agricultural production, local government financial pressure and national food security, Nanchang County, Poyang County, Jianli city and Xiantao City have been listed as China's top grain-producing counties (districts) since 2005 [37].

Nanchang County is located in the southwest of the PYLP, which has been awarded as the National Grain Production Advanced County, National Modern Agriculture Demonstration Area, National Rural Reform Pilot Area, etc. From 1990 to 2020, the agricultural production in Nanchang County had the characteristics of high intensification and agglomeration with the spatial distribution of crop planting, mainly in paddy field rotation. During the 30 years, the average annual planting area of main crops was 0.17 million ha, and the multi-cropping index of cultivated land was 201.67%. The area proportion of rice and rapeseed was 97.16% annually. Only double-cropping rice was the main crop planting structure, accounted for 62.9% of the total cultivated area of main crops, followed by single rice + rapeseed, double-cropping rice + rapeseed, only single rice, with an average annual area proportion of about 10%. Compared with Nanchang County, Poyang County had poor agricultural topographic conditions, with low mountains and hills accounting for 45% of the total area of the county. The degree of intensification and agglomeration of main crop planting was slightly lower. The multi-cropping index averaged 191.41% annually. The area proportion of only double-cropping rice was 43.4%, and the proportion of single rice + rapeseed and only single rice was about 15% annually. The profit of agricultural industry was low, which the added value of the primary industry in the region was only RMB 35,100 Chinese (RMB 47,300 in Nanchang County) in 2019.

Jianli City, located in the middle JHP, was selected as one of the first batch of agricultural modernization demonstration zones of China in 2021. From 1990 to 2020, the average annual planting area of main crops in Jianli City was 0.26 million ha, and the multi-cropping index was 158.23%. The area proportion of rice and rapeseed was 83.32%. The proportion of cultivated land for only single or double-cropping rice was 26.8%. During the past 30 years, the cultivated area of only single rice as well as single rice and rapeseed increased significantly, while the cultivated area of only double-cropping rice and double-cropping rice and rapeseed decreased. Compared with Jianli City, Xiantao City, as a central city in the west wing of the Wuhan metropolitan circle, had rich rural labor resources, high agricultural mechanization, well-equipped facilities and rich profits in its agricultural industry. In 2019, the total power of agricultural machinery was 6.89 kW/ha (5.2 kW/ha in Jianli City), and the added value of the primary industry was RMB 42,700/ha (RMB 37,300/ha in Jianli City). From 1990 to 2020, the area proportion of rice and rapeseed in Xiantao City was 60.25% annually. The area proportions of only single rice or single rice and rapeseed were 25.03% and 14.31% annually, respectively. The area proportions of only double-cropping rice, only maize, maize + rapeseed, soybean + winter wheat were each about 8.5% annually. Compared with Jianli City, the planting structure of main crops in Xiantao City was more diversified, and the areas of paddy field rotation, paddy-upland rotation and dryland rotation were more similar. The planting conditions of cotton and other crops had a greater impact on the overall agricultural production.

As the Hunan Province grain production model area, Dingcheng District of Changde City is a typical area representing the agricultural production characteristics of the DTLF. From 1990 to 2020, the average annual planting area of main crops was 0.12 million ha, and the multi-cropping index was 189.9%. The area proportion of rice and rapeseed was 92.53% annually. The area proportion of only double-cropping rice was higher than that in Jianli City and Xiantao City, though lower than that in Nanchang City and Poyang County, with an annual average of 39.8%, while the cultivated area for only single rice, single rice

and rapeseed, double-cropping rice and rapeseed accounted for about 15% of the annual average while only cotton or cotton and rapeseed accounted for about 6%. In the past 30 years, the proportion of non-agricultural cultivated land in this district (37.8%) was higher than that in the average level of the MYP (29.41%), and the area proportion of cash crops (including cotton and rapeseed) (25.6%) was higher than that in those top grain-producing counties (18.7%). We found the characteristics of crop planting in Dingcheng District directly reflected the results of the interaction between urban economic development and agricultural production development, which was, with the development of economy, the non-grain and non-agricultural phenomenon of cultivated land, becoming more significant.

As one of the areas with the greatest agricultural production potential in the MYP, Qichun County is a typical county representing the agricultural production characteristics of the EHRP. From 1990 to 2020, the planting area of main crops averaged 71,550 ha per year, and the multi-cropping index averaged 173.3%. The area proportion of rice and rapeseed was 63.21% annually. Compared with the above five regions, the area proportion of only single rice or double-cropping rice in this region was closer, accounting for 43% totally. The planting area of single rice and rapeseed, maize and winter wheat accounted for about 10% annually, and the area of only cotton or cotton and rapeseed accounted for about 6% annually. Over the past 30 years, the area of single rice in Qichun County increased from 1280 ha to 14,790 ha, while the area of double-cropping rice decreased from 18,070 ha to 3450 ha. In 2019, the total power of agricultural machinery was only 2.75 kW/ha (the average in the MYP was 5.39 kW/ha). We found that by adjusting the crop-planting structure and improving the degree of agricultural mechanization, the area of crop planting and the intensity of cultivated land use in this county had a great space to increase.

Above all, compared to the DTLF and PYLP, multi-cropping index was larger, the double-cropping rice having smaller advantages, and the conversion to single rice being more prominent in the JHP and EHRP. In addition, the change of planting condition of non-food crops had a relatively great influence on the overall planting condition of main crops. Within each plain, the areas with complex topography or good economic development had worse intensification of main crop planting. In this area, the non-agricultural and non-food conversion of cultivated land was more significant, with the rice and rapeseed planting area smaller and the crop planting structure more complex.

#### 4.2. Potential Driving Forces of Spatio-Temporal Patterns Change of Main Crop Planting

Physical geographical conditions (climate, topography, hydrology, etc.) determine the suitability of crop planting. Water and heat resources had a great influence on main crop intensification planting in the MYP. We found the multiple cropping patterns, whose area accounted for a high proportion, had obvious regional advantages in areas with precipitation higher than 1500 mm and accumulated temperature of 10 °C higher than 5600 °C. Topographic conditions had a great influence on the distribution of crop planting species. For example, rice had a significant geographical advantage in areas with an elevation of less than 25 m, a slope of less than 6°, and a topographic relief of less than 30 m. Compared with the hilly areas of the EHRP and the western JHP, the terrain was flat and suitable for large-scale mechanized cultivation in the DTLF, the PYLP and the middle and eastern JHP, which created positive conditions for intensification, large-scale and agglomeration planting of bulk agricultural products. In the past 30 years, the areas with high intensification, scale and agglomeration of main crops have been mostly distributed in these regions.

The main crop planting trends in the MYP were closely related to agricultural production conditions, agricultural input-output and government policy changes. China's agricultural production moved toward commercialization, specialization and modernization in 1990–2005. During this period, the state's macro-agricultural policies mainly included implementing the grain governor responsibility system, implementing the grain protection price system and reforming the grain circulation system [47]. The agricultural



production conditions in the MYP have been improved constantly. The total power of agricultural machinery has increased from 1.63 kW/ha to 3.32 kW/ha, and the amount of chemical fertilizer has increased from 1.96 kg/ha to 3.44 kg/ha. However, with the rapid development of industrialization and urbanization, the internal incentives of cultivated land property rights have been released, and the response capacity of agricultural production to crops price changes has been enhanced [48], and net profit of agricultural products has presented drastic fluctuation change (Figure 14). At the same time, there was a massive migration of rural labor to cities, with an annual decline of 31,700 in the MYP. The growth of agricultural economy was weak, with the added value of the primary industry on average of only 4.33% in the MYP. Therefore, we found the fluctuation of crop planting profit and the loss of rural labor force in this period resulted in insufficient labor supply in rural areas, which directly led to a significant decrease in crop planting area and the reduction of agricultural intensification, large-scale and agglomeration.

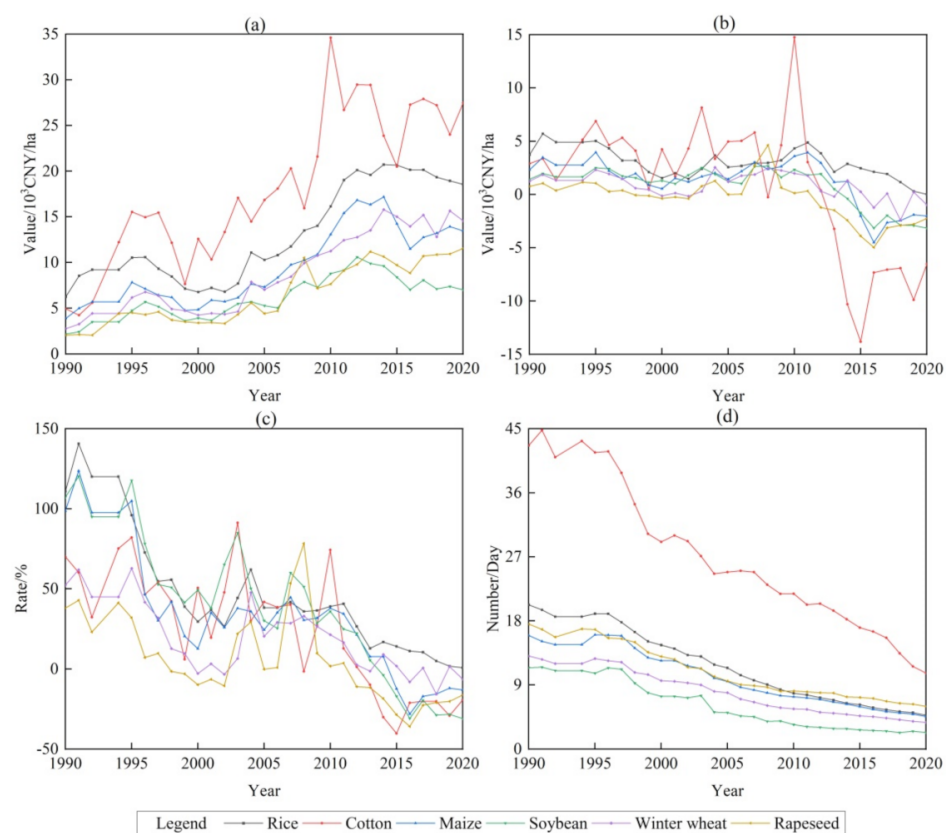


**Figure 14.** Agricultural production costs and benefits in China from 1990 to 2020: (a) the total output value of main crop planting; (b) the net profit value of main crop planting; (c) the net profit rate value of main crop planting; and (d) the number of agricultural workers value of main crop planting.

From 2005 to 2015, China was in a new period of agricultural production development, in which achieving “zero burden” for farmers, breaking the urban-rural dual system and deepening the overall development of urban and rural areas. In 2005, China abolished agricultural taxes in Hunan, Hubei and Jiangxi provinces, implemented policies of incentives for top grain-producing counties, direct subsidy, comprehensive input subsidy, high-quality seed subsidy and agricultural machinery subsidy, and established Policy of Price Floor on Grain as well as the temporary purchase and storage policy [49,50]. China had continuously expanded subsidies for grain production to further protect and mobilize farmers’ enthusiasm for growing grain. Over the past decade, agricultural modernization has been enhanced, and the number of people employed for main crop planting has dropped by about 75 ha/day on average. Agricultural and rural economies were performing well, with the annual growth rate of average primary industry in the MYP rising to 18.36%.

The output value of agricultural products increased significantly and reached its peak around 2015. Especially, the net profit of rice planting was at a high level, reaching RMB 3,175.64/ha. Therefore, during this period, we found farmers' enthusiasm in planting rice, maize and winter wheat have warmed up, and the intensification, large-scale and agglomeration of crop planting have increased accordingly. In addition, cotton, rapeseed and soybean planting conditions in the MYP were also affected by domestic and foreign agricultural trade. With the continuous development of global trade and the widening gap between domestic and foreign prices, the foreign trade deficit of China's oil industry has become increasingly serious, and the soybean and rapeseed planting industries in the MYP have encountered a crisis [51–53]. The mechanization of cotton planting in the Yangtze River Basin has been advanced slowly, resulting in high production cost, large number of labor, low production efficiency and low planting income. Although China implemented temporary purchase and storage policy of cotton in 2011–2014 and rapeseed in 2008–2014, it temporarily protected the profits of cotton and oil farmers but caused high production costs and even worse net profit losses [54,55]. In 2015, China implemented the cotton target price policy in Xinjiang, which further reduced the cotton planting advantage in the MYP [56]. We found that the area and scale of rapeseed, soybean and cotton planting decreased in 2005–2015. Policy interventions combined with falling international prices have increased the price gap between cotton, rapeseed and soybean markets in the MYP and domestic and international markets. Therefore, the fluctuation of agricultural cost and income caused by the implementation of benefit farming policies and the changes of domestic and foreign markets became the main driving factor for the change of crop planting status in the MYP.

China deepened supply-side structural reform in agriculture in 2015–2020. The average gross output value of cultivated crops has shown negative growth as production costs have increased. Except for rice, other main crops showed negative net profit value. The degree of main crop intensification and aggregation planting decreased significantly, the structure of crop planting tended to be diversified, and the phenomenon of non-agricultural and non-food conversion of cultivated land was remarkable in the MYP. We found the effect of agricultural and grain policies on increasing sown area and improving living income has weakened and the degree of main crop intensification and agglomeration planting has decreased in the past five years [57]. However, in order to invigorate rural resources and revitalize rural economy, in addition to increasing investment in agricultural technology and resources, the Chinese government has constantly promoted land consolidation [58] and new agricultural production methods, such as the emerging integrated rice-crawfish farming system [59], and built new types of agricultural management systems, such as specialized large households, family farms, specialized farmer cooperatives and agricultural enterprises that combined intensification, specialization, organization and socialization. We found under the influence of these factors, although farmers were not enthusiastic about planting crops, and the planting area and intensification degree of main crop planting were greatly reduced in the MYP in the past five years, the scale of crop planting was relatively high, with the area proportion of plots exceeding 10 ha being increasing. In addition, the output value of the primary industry on average maintained a medium-high growth rate, with an annual growth rate of 8.83%.

#### 4.3. Uncertainties and Improvement

This study provides an efficient mapping approach and basic information of driving mechanism on the spatio-temporal patterns dynamics change of main crop planting in the MYP in 1990–2020. Based on crop rotation patterns, spectral and phenological characteristics, using the RSPDCM, spatial distribution of main crops in the MYP can be mapped with high accuracy. The ESTARFM is the primary and basic method to process remote sensing data, which was adopted for the fusion of Landsat and MODIS data, and well captured spatial details and vegetation phenological changes of uniform regions, and has high accuracy for heterogeneous and fragmented regions in the MYP. However, the uncertainty of research and its future direction should be recognized. In this study, the classification

and extraction process had a low degree of automation. Cultivated land was generally small and fragmented, so omission classification using Landsat images with 30 m spatial resolution was inevitable. Furthermore, the Google Earth Engine platform could be used to conduct complete time series and large-scale studies with higher spatial resolution. As the existing statistical data at the county (or district) level were short in terms of years and data types, the quantitative driving mechanism could be studied through a questionnaire survey in the future.

In recent years, China has made agricultural production a priority in its agricultural work, ensuring the supply of chemical fertilizer and other agricultural materials and raising the level of agricultural equipment, thus strongly supporting and guaranteeing grain production. Most of the young and middle-aged rural labor force went out for work, and the quality of agricultural labor force declined. The comparative benefit of grain growing was low for a long time, with the contribution of input growth to output being large, and the economic growth mode being mainly extensive [60]. The implementation of national policies has accelerated or slowed down the decline of crop planting area to a certain extent. With the weakening effect of grain subsidies, land consolidation and agricultural large-scale operation become the new reform direction to break through the bottleneck of agricultural productivity and stimulate agricultural vitality.

## 5. Conclusions

As an important grain, cotton and oil production base in China, the spatio-temporal patterns of main crop planting in the MYP changed frequently. Based on the Landsat-MODIS fusion data, we used the RSPDCM to map the planting patterns of the main crops (including rice, cotton, maize, soybean, rapeseed and winter wheat) from 1990 to 2020 (with a time interval of 5 years). Then, we analyzed from the perspectives of overall change trends, intensification, large-scale and agglomeration of spatio-temporal patterns of main crop planting. The results showed that the RSPDCM had good overall accuracy, more than 89%.

From 1990 to 2020, as a high intensification area of main crop planting, mainly in paddy field rotation, the main crop planting area in the MYP showed a trend of dynamic decrease from 6.54 million ha to 3.73 million ha. The annual average of the multi-cropping index was 173.27%, and the annual area proportion of double cropping per year was 63.14%. During the past 30 years, the main crop planting situation in the MYP was divided into three stages, in which the main crop planting showed a continuous downward state in 1990–2005 and 2015–2020, while the main crop planting area showed a temporary upward trend in 2005–2015. The trend of the degree of intensification of main crop planting was basically consistent with that of planting area. As the two most important crops, the increasing and decreasing trend of rice and rapeseed planting area determined the overall change of trend of main crops in the MYP. Rice and rapeseed were also the crops with the highest degree of intensification, large-scale and agglomeration. Large-scale and hot planting areas were mainly distributed in Nanchang and Poyang counties of the PYLP, Anxiang and Yuanjiang counties of the DTLP, and Jianli County of the JHP. In the past five years, due to the proportion of planting area and scale increasing, the substitution effect of maize, soybean and winter wheat on rice and rapeseed was enhanced. The planting hot spots were mainly the JHP and Qichun County, Wuxue City and other places in the EHRP. There were cold spots for crops cultivation around the urban areas, and their intensification, scale and agglomeration declined significantly.

Superior physical and geographical conditions were the basis of agricultural production in the MYP. Hydrothermal conditions directly affected the spatial distribution of cultivated land use intensity, and topographic factors were the main driving factors for the spatial distribution of crop planting. From 1990 to 2020, factors such as labor mobility, agricultural policy and agricultural economic benefits had a great impact on the planting conditions of main crops in the MYP. Our findings contribute to a better understanding of the past dynamic characteristics of main crop cropping patterns in the MYP, which is crucial

for optimizing the allocation of agricultural production resources, managing major grain producing areas and extracting the spatial structure of bulk crops in areas with complex crop rotation patterns by remote sensing.

**Supplementary Materials:** The following supporting information can be downloaded at: <https://www.mdpi.com/article/10.3390/rs14051141/s1>. Table S1: List of available Landsat data from 1989–2020. Figure S1: Spatial distribution of samples verified by remote sensing extraction results of summer and autumn crops in the MYP in 1990–2020. Figure S2: Spatial distribution of samples verified by remote sensing extraction results of overwinter crops in the MYP in 1990–2020.

**Author Contributions:** Conceptualization, L.J. and S.W.; methodology, L.J. and S.W.; software, L.J.; validation, L.J. and S.W.; formal analysis, L.J. and S.W.; investigation, L.J.; resources, L.J., S.W., and Y.L.; data curation, L.J. and S.W.; writing—original draft preparation, L.J. and S.W.; writing—review and editing, L.J. and S.W.; visualization, L.J. and S.W.; supervision, L.J.; project administration, L.J.; funding acquisition, L.J. All authors have read and agreed to the published version of the manuscript.

**Funding:** This research was funded by the National Natural Science Foundation of China, grant number 42071253.

**Institutional Review Board Statement:** Not applicable.

**Informed Consent Statement:** Not applicable.

**Data Availability Statement:** Landsat OLI/TM images are available on the United States Geological Survey (USGS) website (<https://earthexplorer.usgs.gov/>, accessed on 21 March 2021). MOD13Q1 images are available on the National Aeronautics and Space Administration MODIS Data Distribution Center website (<https://modis.gsfc.nasa.gov/>, accessed on 19 May 2021). The administrative division vector data is available on the National Catalogue Service for Geographic Information website (<https://www.webmap.cn/main.do?method=index>, accessed on 10 March 2021). The agrometeorological data is available on the Chinese Meteorological Background dataset website (<https://www.resdc.cn/DOI/doi.aspx?DOIid=39>, accessed on 10 September 2021). The digital elevation data is available on the Shuttle Radar Topography Mission dataset of USGS website ([https://search.earthdata.nasa.gov/search?q=C1546314043-LPDAAAC\\_ECS](https://search.earthdata.nasa.gov/search?q=C1546314043-LPDAAAC_ECS), accessed on 15 September 2021).

**Acknowledgments:** In this section, you can acknowledge any support given which is not covered by the author contribution or funding sections. This may include administrative and technical support, or donations in kind (e.g., materials used for experiments).

**Conflicts of Interest:** The authors declare no conflict of interest.

## References

1. Zhao, H.; Chang, J.; Havlík, P.; van Dijk, M.; Valin, H.; Janssens, C.; Ma, L.; Bai, Z.; Herrero, M.; Smith, P.; et al. China's future food demand and its implications for trade and environment. *Nat. Sustain.* **2021**, *4*, 1042–1051. [\[CrossRef\]](#)
2. Hu, Q.; Xiang, M.; Chen, D.; Zhou, J.; Wu, W.; Song, Q. Global cropland intensification surpassed expansion between 2000 and 2010: A spatio-temporal analysis based on GlobeLand30. *Sci. Total Environ.* **2020**, *746*, 141035. [\[CrossRef\]](#)
3. Liu, Y. Introduction to land use and rural sustainability in China. *Land Use Policy* **2018**, *74*, 1–4. [\[CrossRef\]](#)
4. Su, Y.; Li, C.; Wang, K.; Deng, J.; Shahtahmassebi, A.R.; Zhang, L.; Weijiu, A.; Guan, T.; Pan, Y.; Gan, M. Quantifying the spatiotemporal dynamics and multi-aspect performance of non-grain production during 2000–2015 at a fine scale. *Ecol. Indic.* **2019**, *101*, 410–419. [\[CrossRef\]](#)
5. Erokhin, V.; Gao, T.M. Impacts of COVID-19 on trade and economic aspects of food security: Evidence from 45 developing countries. *Int. J. Environ. Res. Public Health* **2020**, *17*, 5775. [\[CrossRef\]](#) [\[PubMed\]](#)
6. Liu, Y.; Zhou, Y. Reflections on China's food security and land use policy under rapid urbanization. *Land Use Policy* **2021**, *109*, 105699. [\[CrossRef\]](#)
7. Annual Data, Census Data and Regional Data. Available online: <https://data.stats.gov.cn/.Statistics> (accessed on 19 October 2021). (In Chinese)
8. Pan, L.; Xia, H.; Zhao, X.; Guo, Y.; Qin, Y. Mapping winter crops using a phenology algorithm, time-series Sentinel-2 and Landsat-7/8 images, and Google Earth Engine. *Remote Sens.* **2021**, *13*, 2510. [\[CrossRef\]](#)
9. Mulla, D. Twenty five years of remote sensing in precision agriculture: Key advances and remaining knowledge gaps. *Biosyst. Eng.* **2013**, *114*, 358–371. [\[CrossRef\]](#)
10. Tian, H.; Huang, N.; Niu, Z.; Qin, Y.; Pei, J.; Wang, J. Mapping winter crops in China with multi-source satellite imagery and phenology-based algorithm. *Remote Sens.* **2019**, *11*, 820. [\[CrossRef\]](#)



11. Dan, C.A.O.; Feng, J.Z.; Bai, L.Y.; Lan, X.U.N.; Jing, H.T.; Sun, J.K.; Zhang, J. Delineating the rice crop activities in Northeast China through regional parametric synthesis using satellite remote sensing timeseries data from 2000 to 2015. *J. Integr. Agric.* **2021**, *20*, 424–437.
12. Shi, J.; Huang, J.F. Monitoring spatio-temporal distribution of rice planting area in the Yangtze River Delta Region using MODIS images. *Remote Sens.* **2015**, *7*, 8883–8905. [\[CrossRef\]](#)
13. Atzberger, C.; Rembold, F. Mapping the spatial distribution of winter crops at sub-pixel level using AVHRR NDVI time series and neural nets. *Remote Sens.* **2013**, *5*, 1335–1354. [\[CrossRef\]](#)
14. Zhai, Y.; Wang, N.; Zhang, L.; Hao, L.; Hao, C. Automatic crop classification in Northeastern China by improved nonlinear dimensionality reduction for satellite image time series. *Remote Sens.* **2020**, *12*, 2726. [\[CrossRef\]](#)
15. Li, P.; Jiang, L.; Feng, Z.; Sheldon, S.; Xiao, X. Mapping rice cropping systems using Landsat-derived Renormalized Index of Normalized Difference Vegetation Index (RNDVI) in the Poyang Lake Region, China. *Front. Earth Sci.* **2016**, *10*, 303–314. [\[CrossRef\]](#)
16. Yu, B.; Shang, S.H. Multi-year mapping of major crop yields in an irrigation district from high spatial and temporal resolution vegetation index. *Sensors* **2018**, *18*, 3787. [\[CrossRef\]](#)
17. Singha, M.; Wu, B.F.; Zhang, M. An object-based paddy rice classification using multi-spectral data and crop phenology in Assam, Northeast India. *Remote Sens.* **2016**, *8*, 479. [\[CrossRef\]](#)
18. Li, Q.; Wu, B.; Jia, K.; Dong, Q.; Eerens, H.; Zhang, M. Maize acreage estimation using ENVISAT MERIS and CBERS-02B CCD data in the North China Plain. *Comput. Electron. Agric.* **2011**, *78*, 208–214. [\[CrossRef\]](#)
19. Drusch, M.; Del Bello, U.; Carlier, S.; Colin, O.; Fernandez, V.; Gascon, F.; Hoersch, B.; Isola, C.; Laberinti, P.; Matimort, P.; et al. Sentinel-2: ESA's optical high-resolution mission for GMES operational services. *Remote Sens. Environ.* **2012**, *120*, 25–36. [\[CrossRef\]](#)
20. Song, Q.; Hu, Q.; Zhou, Q.; Hovis, C.; Xiang, M.; Tang, H.; Wu, W. In-season crop mapping with GF-1/WFV data by combining object-based image analysis and random forest. *Remote Sens.* **2017**, *9*, 1184. [\[CrossRef\]](#)
21. Lu, L.; Wang, C.; Guo, H.; Li, Q. Detecting winter wheat phenology with SPOT-VEGETATION data in the North China Plain. *Geocarto Int.* **2014**, *29*, 244–255. [\[CrossRef\]](#)
22. Bégué, A.; Arvor, D.; Bellon, B.; Betbeder, J.; De Aballeyra, D.; PDFerraz, R.; Lebourgeois, V.; Lelong, C.; Simoes, M.; RVerón, S. Remote sensing and cropping practices: A review. *Remote Sens.* **2018**, *10*, 99. [\[CrossRef\]](#)
23. You, L.; Wood, S. An entropy approach to spatial disaggregation of agricultural production. *Agric. Syst.* **2006**, *90*, 329–347. [\[CrossRef\]](#)
24. Gao, F.; Masek, J.; Schwaller, M.; Hall, F. On the blending of the Landsat and MODIS surface reflectance: Predicting daily Landsat surface reflectance. *IEEE Trans. Geosci. Remote Sens.* **2006**, *44*, 2207–2218.
25. Hilker, T.; Wulder, M.A.; Coops, N.C.; Linke, J.; McDermid, G.; Masek, J.G.; Gao, F.; White, J.C. A new data fusion model for high spatial- and temporal-resolution mapping of forest disturbance based on Landsat and MODIS. *Remote Sens. Environ.* **2009**, *113*, 1613–1627. [\[CrossRef\]](#)
26. Liao, C.; Wang, J.; Pritchard, I.; Liu, J.; Shang, J. A spatio-temporal data fusion model for generating NDVI time series in heterogeneous regions. *Remote Sens.* **2017**, *9*, 1125. [\[CrossRef\]](#)
27. Filgueiras, R.; Mantovani, E.C.; Fernandes-Filho, E.I.; Cunha, F.F.D.; Althoff, D.; Dias, S.H.B. Fusion of MODIS and Landsat-Like images for daily high spatial resolution NDVI. *Remote Sens.* **2020**, *12*, 1297. [\[CrossRef\]](#)
28. Zhu, X.; Chen, J.; Gao, F.; Chen, X.; Masek, J.G. An enhanced spatial and temporal adaptive reflectance fusion model for complex heterogeneous regions. *Remote Sens. Environ.* **2010**, *114*, 2610–2623. [\[CrossRef\]](#)
29. Griffiths, P.; Nendel, C.; Hostert, P. Intra-annual reflectance composites from Sentinel-2 and Landsat for national-scale crop and land cover mapping. *Remote Sens. Environ.* **2019**, *220*, 135–151. [\[CrossRef\]](#)
30. Song, X.P.; Potapov, P.V.; Krylov, A.; King, L.; Di Bella, C.M.; Hudson, A.; Khan, A.; Adusei, B.; Stehman, S.V.; Hansen, M.C.; et al. National-scale soybean mapping and area estimation in the United States using medium resolution satellite imagery and field survey. *Remote Sens. Environ.* **2017**, *190*, 383–395. [\[CrossRef\]](#)
31. Monfreda, C.; Ramankutty, N.; Foley, J.A. Farming the planet: 2. Geographic distribution of crop areas, yields, physiological types, and net primary production in the year 2000. *Glob. Biogeochem. Cycle* **2008**, *22*, GB1022. [\[CrossRef\]](#)
32. Portmann, F.; Siebert, S.; Doll, P. MIRCA2000-Global monthly irrigated and rainfed crop areas around the year 2000: A new high-resolution data set for agricultural and hydrological modeling. *Glob. Biogeochem. Cycle* **2010**, *24*, 1–24. [\[CrossRef\]](#)
33. Liu, L.; Xu, X.L.; Chen, X. Assessing the impact of urban expansion on potential crop yield in China during 1990–2010. *Food Secur.* **2015**, *7*, 33–43. [\[CrossRef\]](#)
34. Jin, Y.; Liu, X.; Yao, J.; Zhang, X.; Zhang, H. Mapping the annual dynamics of cultivated land in typical area of the Middle-lower Yangtze plain using long time-series of Landsat images based on Google Earth Engine. *Int. J. Remote Sens.* **2020**, *41*, 1625–1644. [\[CrossRef\]](#)
35. Yang, H.; Zhou, J.; Feng, J.; Zhai, S.; Chen, W.; Liu, J.; Bian, X. Ditch-buried straw return: A novel tillage practice combined with tillage rotation and deep ploughing in rice-wheat rotation systems. In *Advances in Agronomy*; Academic Press: Cambridge, MA, USA, 2019; Volume 154.
36. Zuo, L.; Wang, X.; Zhang, Z.; Zhao, X.; Liu, F.; Yi, L.; Liu, B. Developing grain production policy in terms of multiple cropping systems in China. *Land Use Pol.* **2014**, *40*, 140–146. [\[CrossRef\]](#)

37. Ministry of Finance of China. Notice on printing and distributing the Interim Measures for the Administration of Reward Funds in Major Grain (Oil) Producing Counties. Available online: [http://www.mof.gov.cn/zhuantihuigu/cczqzyzfglbf/ybxzyzf\\_7774/cldxjlzj\\_7777/201810/t20181010\\_3042371.htm](http://www.mof.gov.cn/zhuantihuigu/cczqzyzfglbf/ybxzyzf_7774/cldxjlzj_7777/201810/t20181010_3042371.htm) (accessed on 10 October 2021). (In Chinese)
38. Tao, J.; Wu, W.; Liu, W.; Xu, M. Exploring the spatio-temporal dynamics of winter rape on the Middle Reaches of Yangtze River Valley using time-series MODIS data. *Sustainability* **2020**, *12*, 466. [CrossRef]
39. Rouse, J.W.; Haas, R.S.; Schell, J.A.; Deering, D.W. *Monitoring Vegetation Systems in the Great Plains with ERTS*; NASA: Washington, DC, USA, 1973; pp. 309–317.
40. Huete, A.; Didan, K.; Miura, T.; Rodriguez, E.P.; Gao, X.; Ferreira, L.G. Overview of the radiometric and biophysical performance of the MODIS vegetation indices. *Remote Sens. Environ.* **2002**, *83*, 195–213. [CrossRef]
41. Xu, H. A study on information extraction of water body with the modified normalized difference water index (MNDWI). *J. Remote Sens.* **2005**, *9*, 589–595. (In Chinese)
42. Hatfield, J.; Prueger, J.H. Value of using different vegetative indices to quantify agricultural crop characteristics at different growth stages under varying management practices. *Remote Sens.* **2010**, *2*, 562–578. [CrossRef]
43. Cassman, K. Ecological intensification of cereal production systems: Yield potential, soil quality, and precision agriculture. *Proc. Natl. Acad. Sci. USA* **1999**, *96*, 5952–5959. [CrossRef]
44. Xu, Y.; Li, X.; Xin, L. Differentiation of scale-farmland transfer rent and its influencing factors in China. *Acta Geogr. Sin.* **2021**, *76*, 753–763. (In Chinese)
45. ArcMap Help–ArcToolbox. Available online: <http://www.esri.com/> (accessed on 19 October 2021).
46. Wang, X.; Chen, Y.; Sui, P.; Gao, W.; Qin, F.; Zhang, J.; Wu, X. Emergy analysis of grain production systems on large-scale farms in the North China Plain based on LCA. *Agric. Syst.* **2014**, *128*, 66–78. [CrossRef]
47. Decision of The State Council on Further Deepening Reform of Grain Circulation System. Available online: [http://www.moa.gov.cn/gk/zcfg/xzfg/200601/t20060123\\_540354.htm](http://www.moa.gov.cn/gk/zcfg/xzfg/200601/t20060123_540354.htm) (accessed on 19 November 2021). (In Chinese)
48. Chari, A.; Liu, E.M.; Wang, S.Y.; Wand, Y. Property rights, land misallocation, and agricultural efficiency in China. *Rev. Econ. Stud.* **2021**, *88*, 1831–1862. [CrossRef]
49. Regulations on the Administration of Grain Circulation. Available online: [http://www.moa.gov.cn/gk/zcfg/xzfg/200601/t20060123\\_541832.htm](http://www.moa.gov.cn/gk/zcfg/xzfg/200601/t20060123_541832.htm) (accessed on 20 November 2021). (In Chinese)
50. Yi, F.; Sun, D.Q.; Zhou, Y.H. Grain subsidy, liquidity constraints and food security—impact of the grain subsidy program on the grain-sown areas in China. *Food Policy* **2015**, *50*, 114–124. [CrossRef]
51. Yan, H.; Chen, Y.Y.; Ku, H.B. China’s soybean crisis: The logic of modernization and its discontents. *J. Peasant Stud.* **2016**, *43*, 373–395.
52. Sun, J.; Yang, L.; Zhao, F.Q.; Wenbin, W. Domestic dynamics of crop production in response to international food trade: Evidence from soybean imports in China. *J. Land Use Sci.* **2020**, *15*, 91–98. [CrossRef]
53. Sun, J.; Mooney, H.; Wu, W.; Tang, H.; Tong, Y.; Xu, Z.; Huang, B.; Cheng, Y.; Yang, X.; Wei, D.; et al. Importing food damages domestic environment: Evidence from global soybean trade. *Proc. Natl. Acad. Sci. USA* **2018**, *115*, 5415–5419. [CrossRef]
54. Notice on the Acquisition of Rapeseed in 2009. Available online: [http://www.gov.cn/govweb/gongbao/content/2009/content\\_1407886.htm](http://www.gov.cn/govweb/gongbao/content/2009/content_1407886.htm) (accessed on 25 November 2021).
55. Temporary Purchase and Storage of Cotton in 2011–2014. Available online: <http://www.gov.cn/> (accessed on 26 November 2021). (In Chinese)
56. National Development and Reform Commission of China; Ministry of Finance of China; Ministry of Agriculture of China. Xinjiang Launched Trials to Subsidize Target Prices for Cotton and Abolished the Temporary Purchase and Storage Policy. Available online: [http://www.gov.cn/xinwen/2014-04/12/content\\_2657725.htm](http://www.gov.cn/xinwen/2014-04/12/content_2657725.htm) (accessed on 12 October 2021). (In Chinese)
57. Huang, J.; Yang, G.L. Understanding recent challenges and new food policy in China. *Glob. Food Secur.-Agric. Policy* **2016**, *12*, 119–126. [CrossRef]
58. Opinions on Guiding Orderly Transfer of Rural Land Management Rights to Develop Moderate Scale Agricultural Operations. Available online: [http://www.gov.cn/xinwen/2014-11/20/content\\_2781544.htm](http://www.gov.cn/xinwen/2014-11/20/content_2781544.htm) (accessed on 27 November 2021). (In Chinese)
59. Wei, Y.; Lu, M.; Yu, Q.; Xie, A.; Hu, Q.; Wu, W. Understanding the dynamics of integrated rice–crawfish farming in Qianjiang county, China using Landsat time series images. *Agric. Syst.* **2021**, *191*, 103167. [CrossRef]
60. Gong, B. Agricultural reforms and production in China: Changes in provincial production function and productivity in 1978–2015. *J. Dev. Econ.* **2018**, *132*, 18–31. [CrossRef]